FIELD STUDY OF WAVE TRANSMISSION THROUGH A RUBBLE-MOUND BREAKWATER

by

Ronald Joel Calhoun

United States
Naval Postgraduate School

THESIS

FIELD STUDY OF WAVE TRANSMISSION
THROUGH A RUBBLE-MOUND BREAKWATER

by

Ronald Joel Calhoun

Thesis Advisor: E. B. Thornton

March 1971

Approved for public release; distribution unlimited.

Field Study of Wave Transmission Through a Rubble-Mound Breakwater

by

Ronald Joel Calhoun
Lieutenant Commander, United States Navy
B.S., Naval Academy, 1963

Submitted in partial fulfillment of the
requirements for the degree of

MASTER OF SCIENCE IN OCEANOGRAPHY

from the

NAVAL POSTGRADUATE SCHOOL
March 1971

ABSTRACT

Characteristics of sea and swell incident at a permeable rubble-mound breakwater located in Monterey Harbor, California, are resolved into reflected and transmitted components. The wave characteristics are studied by analyzing synchronized wave records of three underwater sensors judiciously placed, two to seaward and one to landward of the breakwater. Power spectra and cross spectra are calculated for various characteristic sea states selected from three months of observations. Amplitude and phase are determined for the spectral wave components comprising the partial standing wave phenomena. This study was unique in that it entails experiments conducted in the field on a prototype structure in the natural environment. Transmission has been studied heretofore exclusively with scale models. The coefficients of transmission are considerably less for the prototype than predicted by a Corps of Engineers model study of the Monterey Breakwater. The differences are apparently related to more wave energy scattering and dissipation due to turbulence than predicted by the model.

TABLE OF CONTENTS

LIST OF FIGURES

LIST OF TABLES

ACKNOWLEDGEMENTS

The author wishes to express his sincere appreciation to Dr. Edward B. Thornton of the Department of Oceanography, Naval Postgraduate School, under whose direction this thesis was written. His encouragement, criticism, recommendations, and experience were invaluable in the completion of this research. Special thanks are also given to Professor Warren C. Thompson for critically reading the manuscript.

In addition, the author is indebted to Mr. Robert C. Smith, Research Technician with the Department of Research Administration, for his valuable assistance in calibrating and preparing the wave sensors for operation, and to Mr. Jack C. Mellor, Oceanographer with the Department of Oceanography, for his technical advice and assistance in installing the wave sensors.

I. INTRODUCTION

A. BACKGROUND

1. Monterey Harbor

Monterey Harbor (Figure 1) is located at the southern end of Monterey Bay about 75 nautical miles south of San Francisco, California. The Bay is a large symmetric, crescent-shaped, open embayment approximately 22 nautical miles long from north to south, nine nautical miles wide, and is slightly closed at its extreme northern and southern ends by two stubby land masses (Figure 2). A unique feature of the bay is the deep Monterey Submarine Canyon which divides the bay roughly into two halves. The submarine canyon is one of the largest in the world, and it exerts significant influences on both directional and height characteristics of waves within the bay.

Until the 1940's the harbor's primary function was to provide an anchorage haven for fishing fleets. However, due to the reduced fish catch in recent years, the activities of the harbor have been largely reoriented to recreational boating and tourist attraction features including sports fishing. In 1934, a rubble-mound breakwater was constructed to provide harbor protection for the expanding fishing industry. It soon became evident that this structure did not provide sufficient mooring area for the growing number of fishing and small craft, nor did it provide adequate protection from wave and surge action. Current plans include construction of additional breakwater structures to provide a larger and safer anchorage for small craft.

Long-period waves occurring in the bay at times cause a substantial surge in the harbor. In addition, the harbor is exposed to

(View looking west)

(View looking northwest)

FIGURE 1

Monterey Harbor

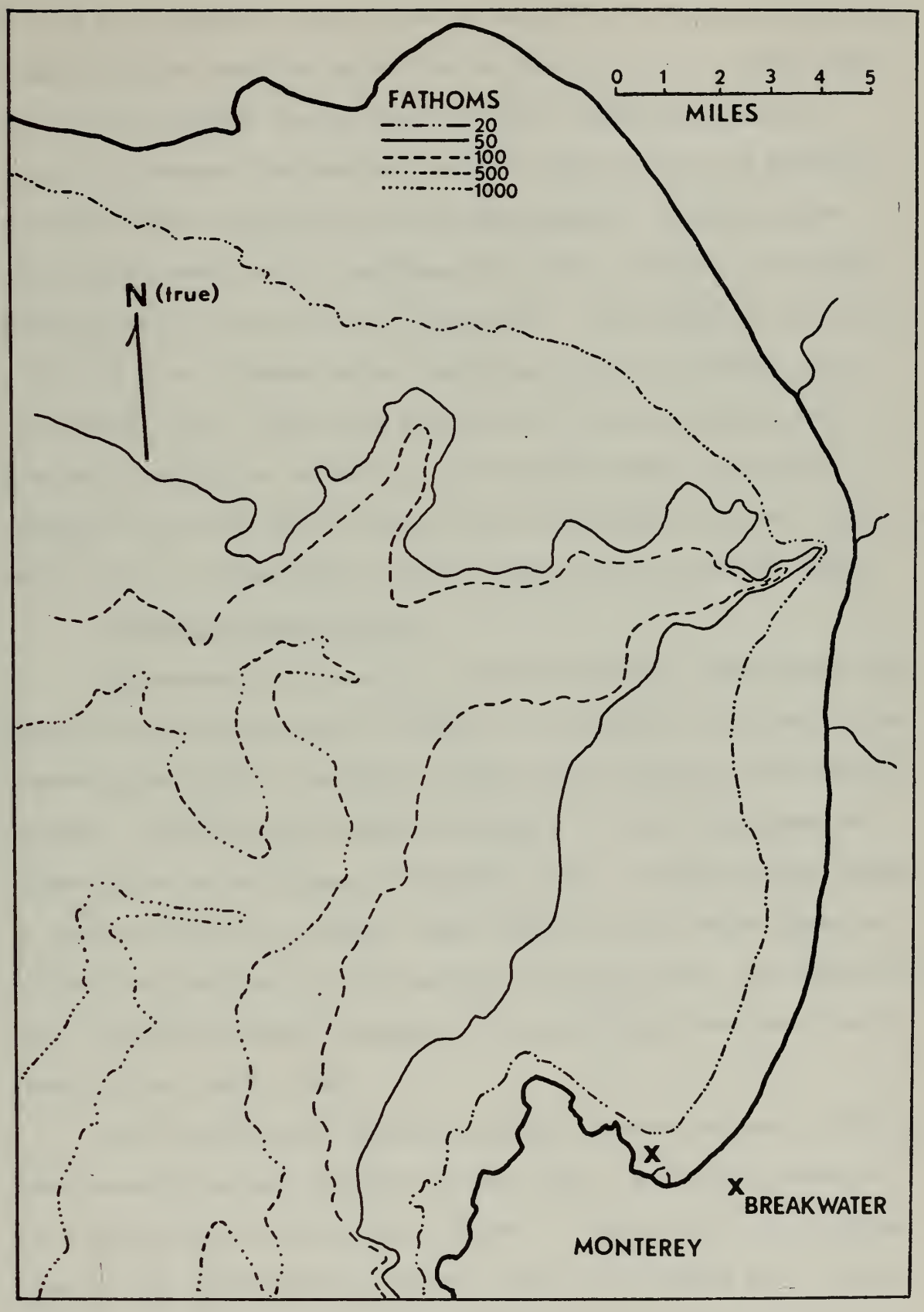

FIGURE 2

Monterey Bay

sea and swell arriving from outside the bay from the deepwater directions between west and north-northwest, and on rare occasions to local winds from the north within the bay [Bixby, 1962]. Refraction diagrams (Figure 3) obtained from the San Francisco District Corps of Engineers show that waves entering the bay from the deepwater directions from approximately west to north-northwest (260 deg to 332 deg) are almost unidirectional in the vicinity of the harbor. These waves are often of sufficient size to damage harbor facilities as well as fishing boats and pleasure craft. There have been several studies concerned with wave and surge effects on the bay and the harbor which have led to analytical solutions and hydraulic model investigations [Hudson, 1949; Wilson, Hendrickson and Kilmer, 1965; Chatham, 1968; Bucci and Whalin, 1969].

2. Breakwater Characteristics

The Monterey structure is a typical permeable, rubble-mound type preferred for coastal harbors because it is economical, adaptable to any reasonable water depth, suitable on nearly all foundations, and readily repaired. Rubble-mound breakwaters are more or less a heterogeneous assemblage of natural stones of different sizes and shapes either dumped at random or placed in courses. Side slopes and armor stone sizes are designed to effectively resist the expected wave action. The rubble-mound type is used extensively throughout the United States and almost exclusively on the Pacific Coast.

The first Monterey Harbor breakwater construction was a 1300-foot rubble-mound structure completed in early 1934. A 400-foot extension was completed late the same year (Figure 4). The crest is at elevation plus ten feet (MLLW) and is 15 feet in width. The harbor side slope is one and one-half horizontal on one vertical for the full length of the

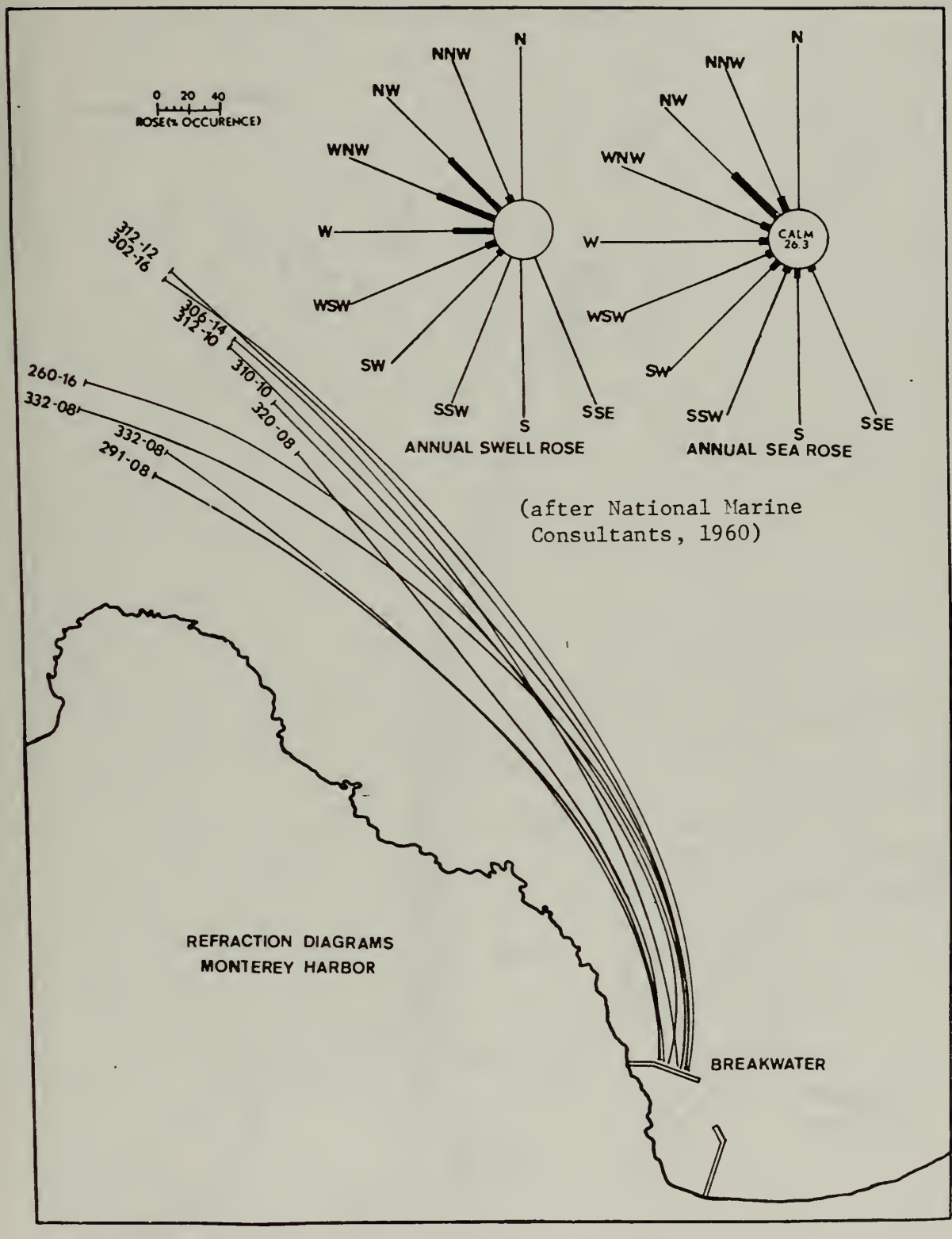

FIGURE 3

Monterey Harbor Refraction Diagrams

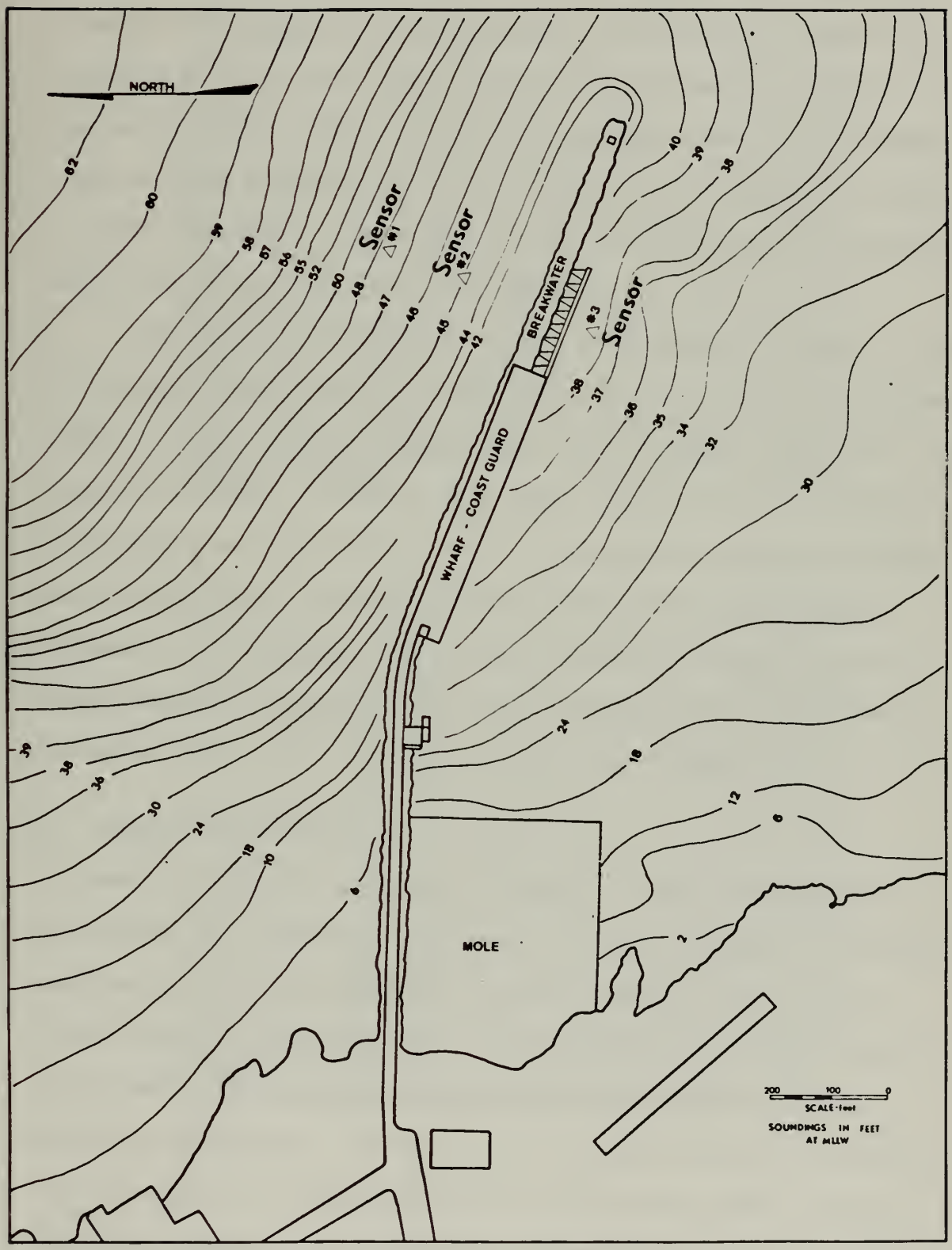

FIGURE 4

Monterey Breakwater

breakwater. The seaward side slope is one and one-half horizontal on one vertical for the original 1300 feet. The 400-foot extension has a seaward side slope of one and one-half on one vertical from crest to elevation minus 16 feet (MLLW), and one and one-quarter horizontal on one vertical below that depth. The structural adequacy of the breakwater has been substantiated by the fact that no replacement of stone or other preventative maintenance has been required since it was built, and it has remained a stable configuration.

The Monterey breakwater consists of an interior section, or core, of assorted sizes of stone, gravel, and fines, protected by a ten-foot layer of coarse, angular-shaped armor cover components (Figure 5). The exterior A stones, or primary cover layer, placed to attain an interlocking fit, are approximately ten tons per rubble component for the original 1300 feet, and four to twelve tons each for the 400-foot extension. The original 1300 feet has a cement cap roadway laid in conjunction with the construction of a wharf and mooring dolphins on the harbor side. The breakwater has never been grouted.

B. PROBLEM AND APPROACH

When sea and swell impinge upon sloping permeable rubble-mound structures, they may break, and thereby dissipate energy by turbulence, they may be reflected to produce a partial standing wave by interference with the incident waves, and they may be transmitted through or partially over the structure with energy loss due to turbulence within the breakwater. The resulting interplay of forces developed by the wave-induced water motions and the action of the rubble units is extremely complex due to the variable reflective and friction properties of the sloping face and the general characteristic roughness of the

FIGURE 5

Monterey Breakwater Structure

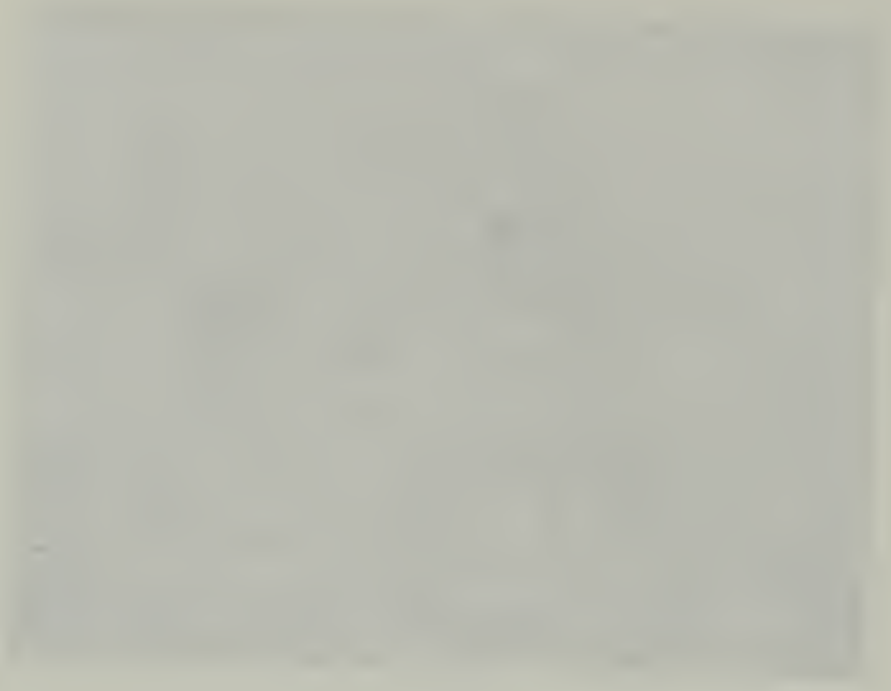

interior of the permeable structure. Attempts to determine by theoretical analysis the hydrodynamic characteristics related to stability and transmission have not been productive.

The problem of determining wave transmission was surmounted in this study by application of the principal of energy conservation to statistical wave observations. This was done by measuring the wave motion in the field with wave sensors judiciously placed on both sides of a permeable breakwater. Wave components were computed through spectral analysis of the individual wave records. Reflected and incident wave components were determined through application of linear wave theory for each frequency bandwidth. The transmitted wave component was computed from measurement of the progressive wave in the lee of the breakwater. The energy dissipated was then quantitatively deduced by determining the difference between the incident wave energy and the reflected and transmitted wave energy.

Sample wave records from this particular wave field were considered accurate estimates of an ergodic, stationary, random process. Conversion of these finite sample time histories to a spectral density (frequency) representation was accomplished through computer analysis. Fourier analysis was used to break down the random sea process into simple sinusoidal harmonic components whose behavior was analyzed by the use of classical linear theories of wave motion.

C. OBJECTIVE

The objective of this investigation is threefold, and can be conveniently separated to include the following areas of interest:

1. Investigate the feasibility of determining the incident and reflected components on the incident side of a permeable breakwater through selective placement of wave sensors in the field.

2. Consider the wave-transmission problem as a stochastic process as opposed to consideration of monochromatic waves; utilize spectral analysis to resolve the random sea environment into a continuum of wave components described by linear wave theory for a specified range of frequencies; and compute transmitted and reflected wave coefficients and the energy dissipation of the breakwater from equations derived from linear wave theory.

3. Compare the results of this field study with hydraulic model transmission tests of the combination tribar, rubble-mound breakwater proposed for Monterey Harbor by Davidson [1969].

II. THEORETICAL CONSIDERATIONS

A. WAVE DESCRIPTION

The sea and swell selected for this study arrived incident at Monterey Harbor approximately normal to the breakwater (Figure 3). The areas adjacent to the breakwater are fairly uniform in depth. It is assumed that these random sea and swell waves can be analyzed as the result of the superposition of a number of component sinusoidal (Airy) wave trains with their own characteristic height, frequency, direction, and random phase. For incident waves of low steepness at the depths involved in this study, Airy theory was shown by Dean [1968] to give a reasonably valid approximation. These considerations are extended to random sea theory. The linear wave theory problem for a partially reflected wave is presented below. The linear solutions are then superimposed to obtain the spectrum of the actual sea surface.

B. WAVE AMPLITUDES

The incident and reflected wave amplitudes are computed by considering two progressive waves moving in opposite directions comprising a system of imperfect or partial reflecting waves (Figure 6). Basic assumptions include: monochromatic and long-crested waves, wave direction normal to the breakwater, and a horizontal seabed. Assuming linear theory, the incoming and reflected components of the wave surface elevation, η, can be superimposed as follows,

$$\eta_1 = \eta_I + \eta_R = a_I \cos(kx_1 - \sigma t + \delta_I) + a_R \cos(kx_1 + \sigma t + \delta_R) \tag{1.1}$$

$$\eta_2 = \eta_I + \eta_R = a_I \cos(kx_2 - \sigma t + \delta_I) + a_R \cos(kx_2 + \sigma t + \delta_R) \tag{1.2}$$

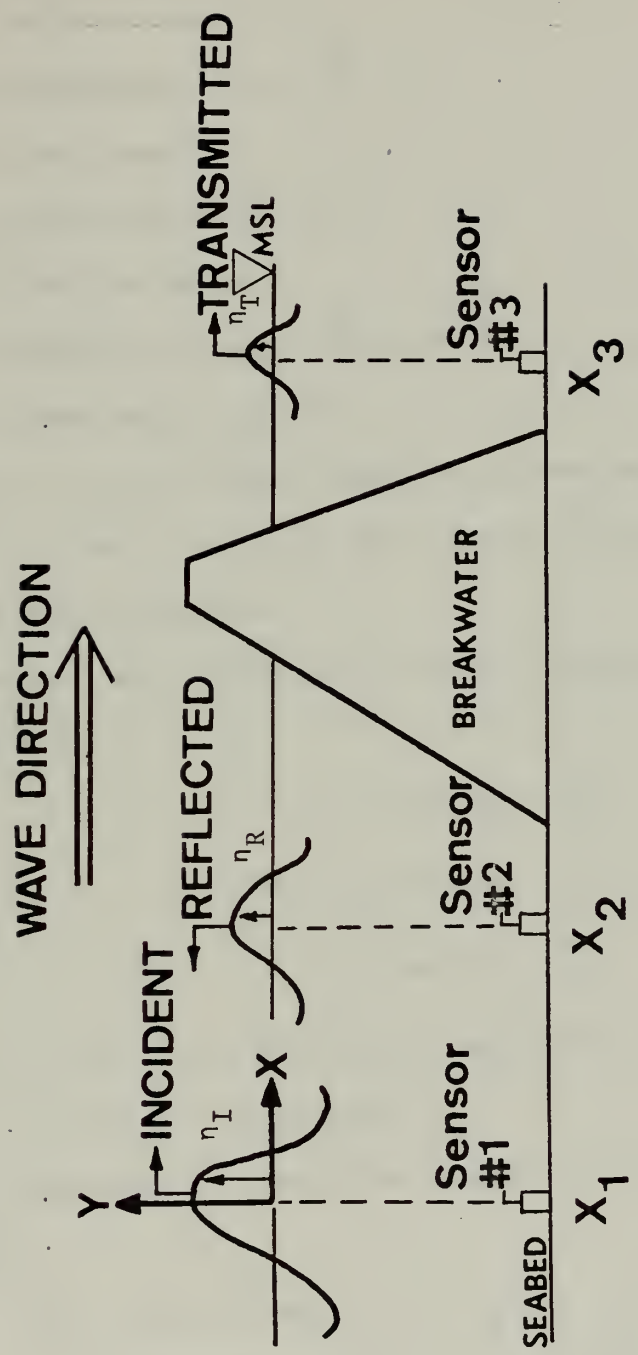

FIGURE 6

Transmission through a Permeable Breakwater

where,

H = height of wave, ft.

a = amplitude of wave $(\frac{H}{2})$, ft.

L = wave length, ft.

k = wave number $(\frac{2\pi}{L})$, ft^{-1}.

T = wave period, sec.

σ = angular frequency $(\frac{2\pi}{T})$, sec^{-1}.

δ = phase angle, degrees.

Subscripts 1, 2, and 3 denote quantities corresponding to wave sensors numbered 1, 2, and 3; and I, R, and T refer to incident, reflected, and transmitted wave components.

The measured statistical values of sea surface elevation from the wave sensors are,

$$\eta_1 = A_1 \cos (\sigma t - \delta_1) \tag{1.3}$$

$$\eta_2 = A_2 \cos (\sigma t - \delta_2) \tag{1.4}$$

$$\eta_3 = a_T \cos (\sigma t - \delta_3) \tag{1.5}$$

where A_1, A_2, and a_T are statistical amplitudes measured at wave sensors numbered 1, 2, and 3, respectively.

Using trigonometric identities, equations (1.1) and (1.2) are expanded as,

$$\begin{aligned}\eta_1 = {} & [a_I \cos (kx_1 + \delta_I) + a_R \cos (kx_1 + \delta_R)] \cos \sigma t \\ & + [a_I \sin (kx_1 + \delta_I) - a_R \sin (kx_1 + \delta_R)] \sin \sigma t\end{aligned} \tag{1.6}$$

$$\begin{aligned}\eta_2 = {} & [a_I \cos (kx_2 + \delta_I) + a_R \cos (kx_2 + \delta_R)] \cos \sigma t \\ & + [a_I \sin (kx_2 + \delta_I) - a_R \sin (kx_2 + \delta_R)] \sin \sigma t\end{aligned} \tag{1.7}$$

Similarly, trigonometric expansion of equations (1.3) and (1.4) yield,

$$\eta_1 = A_1 (\cos \sigma t \cos \delta_1 + \sin \sigma t \sin \delta_1) \tag{1.8}$$

$$\eta_2 = A_2 (\cos \sigma t \cos \delta_2 + \sin \sigma t \sin \delta_2) \tag{1.9}$$

Equating coefficients of cos σt and sin σt of the measured and theoretical values of η_1 and η_2 introduces the relationships,

$$A_1 \cos \delta_1 = a_I \cos (kx_1 + \delta_I) + a_R \cos (kx_1 + \delta_R) \tag{1.10}$$

$$A_1 \sin \delta_1 = a_I \sin (kx_1 + \delta_I) - a_R \sin (kx_1 + \delta_R) \tag{1.11}$$

$$A_2 \cos \delta_2 = a_I \cos (kx_2 + \delta_I) + a_R \cos (kx_2 + \delta_R) \tag{1.12}$$

$$A_2 \sin \delta_2 = a_I \sin (kx_2 + \delta_I) - a_R \sin (kx_2 + \delta_R) \tag{1.13}$$

Rewriting equations (1.10) and (1.11) using trigonometric identities yields,

$$A_1 \cos \delta_1 = a_I (\cos kx_1 \cos \delta_I - \sin kx_1 \sin \delta_I) + a_R (\cos kx_1 \cos \delta_R - \sin kx_1 \sin \delta_R) \tag{1.14}$$

$$A_1 \sin \delta_1 = a_I (\sin kx_1 \cos \delta_I + \cos kx_1 \sin \delta_I) - a_R (\sin kx_1 \cos \delta_R + \cos kx_1 \sin \delta_R) \tag{1.15}$$

Rearranging terms,

$$A_1 \cos \delta_1 = \cos kx_1 (a_I \cos \delta_I + a_R \cos \delta_R) - \sin kx_1 (a_I \sin \delta_I + a_R \sin \delta_R) \tag{1.16}$$

$$A_1 \sin \delta_1 = \cos kx_1 (a_I \sin \delta_I - a_R \sin \delta_R) + \sin kx_1 (a_I \cos \delta_I - a_R \cos \delta_R) \tag{1.17}$$

Similarly rewriting equations (1.12) and (1.13) using trigonometric expansion yields,

$$A_2 \cos \delta_2 = \cos kx_2 (a_I \cos \delta_I + a_R \cos \delta_R) - \sin kx_2 (a_I \sin \delta_I + a_R \sin \delta_R) \tag{1.18}$$

$$A_2 \sin \delta_2 = \cos kx_2 (a_I \sin \delta_I - a_R \sin \delta_R) + \sin kx_2 (a_I \cos \delta_I - a_R \cos \delta_R) \tag{1.19}$$

Judiciously choosing the origin of x at wave sensor No. 1 sets quantity x_1 equal to zero. Further, since phase angles are relative quantities, δ_1 is set equal to zero which redefines δ_2 as the phase difference, henceforth denoted as δ. Thus equations (1.16) and (1.17) are further simplified to yield,

$$A_1 = a_I \cos \delta_I + a_R \cos \delta_R \tag{1.20}$$

$$0 = a_I \sin \delta_I - a_R \sin \delta_R \tag{1.21}$$

Substitution of equations (1.20) and (1.21) into (1.18) and (1.19) yields,

$$A_2 \cos \delta = A_1 \cos kx_2 - 2a_R \sin kx_2 \sin \delta_R \tag{1.22}$$

$$A_2 \sin \delta = A_1 \sin kx_2 - 2a_R \sin kx_2 \cos \delta_R \tag{1.23}$$

Solving for $\sin \delta_R$ and $\cos \delta_R$ in equations (1.22) and (1.23) and dividing yields,

$$\delta_R = \tan^{-1} \left[\frac{A_1 \cos kx_2 - A_2 \cos \delta}{A_1 \sin kx_2 - A_2 \sin \delta} \right] \tag{1.24}$$

Solving for a_R in equation (1.22) in terms of δ_R gives,

$$a_R = \frac{-A_2 \cos \delta + A_1 \cos kx_2}{2 \sin kx_2 \sin \delta_R} \tag{1.25}$$

Utilizing equations (1.20) and (1.21) and dividing gives the solution for δ_I in terms of δ_R and a_R as,

$$\delta_I = \tan^{-1} \left[\frac{a_R \sin \delta_R}{A_1 - a_R \cos \delta_R} \right] \tag{1.26}$$

Solving for a_I from equation (1.21) gives the solution for a_I in terms of δ_I, δ_R, and a_R yields,

$$a_I = \frac{a_R \sin \delta_R}{\sin \delta_I} \tag{1.27}$$

C. WAVE REFLECTION AND TRANSMISSION COEFFICIENTS

The quantities a_R and a_I have been evaluated in terms of known or measurable quantities A_1, A_2, k, x_2 and δ. The reflection coefficient, K_R, and transmission coefficient, K_T, are defined as,

$$K_R = \frac{a_R}{a_I} \tag{1.28}$$

$$K_T = \frac{a_T}{a_I} \tag{1.29}$$

and can therefore be evaluated using computed values a_R, a_I, and measured quantity a_T.

D. WAVE ENERGY DISSIPATION

The average power per unit length of wave crest can be expressed analytically as the average time rate of change of energy within an element of fluid through which the wave passes. The power dissipated by the breakwater can be computed by writing an expression equating the power incident on the breakwater, the power transmitted through the breakwater, and the power reflected from the breakwater. The equation for a power balance for both the seaward and the harbor side of the breakwater may be written as,

$$\gamma \frac{a_I^2}{2} C_{G_I} - \gamma \frac{a_T^2}{2} C_{G_T} - \gamma \frac{a_R^2}{2} C_{G_R} = P_D \tag{1.30}$$

where,

γ = specific weight of sea water, 64.0 lb/ft^3.

C_G = wave group velocity, ft/sec.

P_D = power dissipated, ft-lb/sec per ft of wave crest.

Assuming constant depth for simplification and rewriting the terms in equation (1.30) yields,

$$C_{G_I} = C_{G_R} = C_{G_T} = C_G, \text{ and} \tag{1.31}$$

$$K_E = \frac{P_D}{\gamma\, a_I^2/C_G} = 1 - \left(\frac{a_T}{a_I}\right)^2 - \left(\frac{a_R}{a_I}\right)^2 \tag{1.32}$$

Using previously defined notation yields,

$$K_E = 1 - K_T^2 - K_R^2 \tag{1.33}$$

where,

K_E = coefficient of energy dissipation expressed as the fraction of the incident wave power dissipated.

The simplifying assumption of constant depth is justified to seaward of the breakwater. The depth changes from 47 feet at the seaward sensor (No. 1) to 42 feet at the toe of the breakwater (Figure 4). The depth decreases from an average of 46 feet for the two seaward sensors (No. 1 and No. 2) to 39 feet at the harbor sensor (No. 3). The assumption of a constant depth bottom of 46 feet results in a maximum error for the transmitted energy of less than eight per cent for a 20-second wave, the error decreasing with decreasing period, and so will be used in the analysis.

III. ANALYTICAL PROCEDURE

A. SEAWARD WAVE DATA

The wave records to seaward of the breakwater are rectilinear analog traces measured with two identical sensors. These records were digitized at 100 points to the inch using a Calma Company Model 480 mechanical digitizer and interpreted by program CONVERT [Lynch, 1970] using the CDC 6500 computer at Fleet Numerical Weather Central, Monterey. A record length of 2048 points was digitized with a sampling interval of 0.63 seconds for a time record of 0.358 hours or approximately 21.5 minutes. This corresponds to approximately 250 oscillations of the average period wave which is generally considered a reliable base sample for analysis of ocean wave records. The sensors eliminate tidal, seiche, and other long-period influences through high-pass filtering by hydraulic means inherent in the pressure differential transducers (time constants 47 and 50 seconds). Possible electronically generated direct-current drift was removed by computing the linear trend and correcting the individual raw data points.

B. HARBOR WAVE DATA

The wave records from the harbor side of the breakwater are curvilinear analog traces measured with a single sensor. Although a differential pressure transducer of different design than the seaward wave sensors was used, high-pass filtering was similarly accomplished by hydraulic filtering (time constant 60 seconds). The raw data were corrected for linear trends using the same procedure as for the seaward data.

As previously stated, the harbor wave data were recorded on curvilinear coordinates. The Calma 480 digitizer accepts rectilinear coordinates which resulted in additional problems in data reduction. These records were analyzed at 100 points to the inch, but at a sampling interval of 0.80 seconds. A record length of 2048 points was digitized for a time record of 0.455 hours, or approximately 27.3 minutes. The unadjusted amplitudes and time increments obtained from the digitizer and computer program CONVERT were recorded in incremental paths every 0.01 inch of stylus travel. The rectilinear coordinates from the digitizer were then converted to the approximately correct curvilinear coordinates (t, $R\theta$) by employing geometric relationships as follows (Figure 7),

$$t_i = x_i + R - \sqrt{R^2 - y_i^2} \text{ , and} \tag{3.1}$$

$$\theta_i = \tan^{-1} \frac{y_i}{\sqrt{R^2 - y_i^2}}$$

where,

t_i = time in curvilinear coordinates.

R = radius of curvature for arcs of constant t_i.

y_i = the ordinate on the cartesian scale.

x_i = time scale in equally spaced increments of t on the rectangular cartesian scale.

The adjusted heights are then computed as,

$$y_i = R\theta_i \tag{3.2}$$

where y_i is now the adjusted wave surface elevation value. Since the space increment is 0.01 inch, the adjusted time, t_i, is,

$$t_i = 80\ x_i \tag{3.3}$$

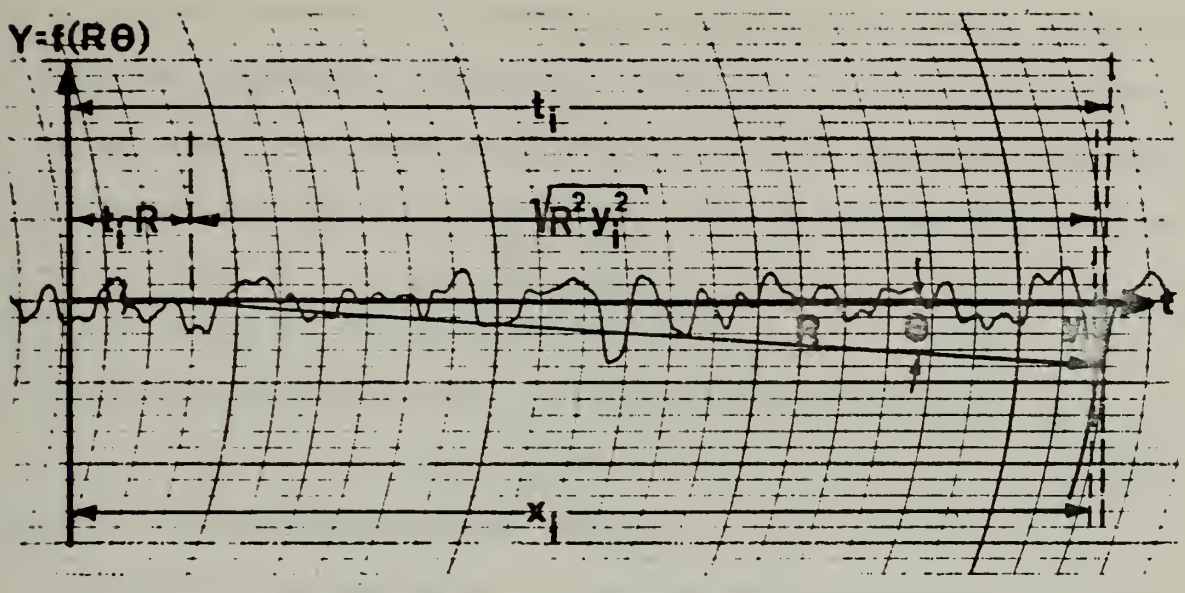

FIGURE 7

Geometric Relationships for Conversion from Curvilinear Coordinates (R,θ) to Rectilinear Coordinates (y,t).

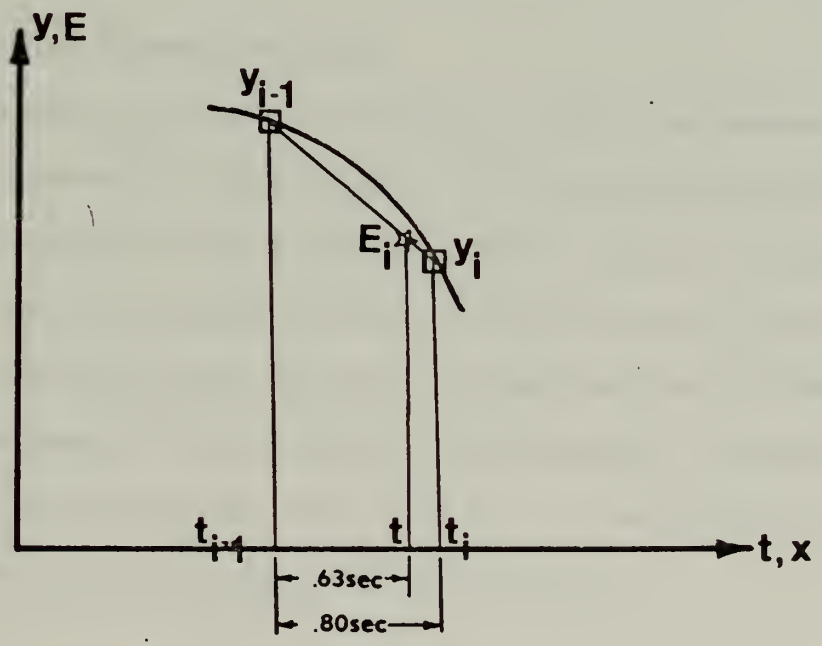

FIGURE 8

Linear Interpolation

A linear interpolation scheme is then performed to match the seaward data time increments. The computer checks each successive time value of the harbor wave record and interpolates to the appropriate increment of the uniform sampling interval. The slope of the line (Figure 8) is,

$$\frac{\Delta y}{\Delta t} = \frac{(y_i - y_{i-1})}{(t_i - t_{i-1})} \tag{3.4}$$

The horizontal spatial scale for the interpolated values is,

$$x_i = (i-1)\Delta \tag{3.5}$$

where Δ = the uniform sampling interval.

This final interpolation to a uniform sampling interval, Δ, is a critical step in curvilinear to rectilinear coordinates conversion. Although not a requirement in the analysis, all the wave data are then of the same sampling interval of 0.63 seconds of wave time.

C. COMPUTATION OF POWER SPECTRUM

The analysis of the digital records is made in accordance with the method of Blackman and Tukey [1958] with the computations performed on an IBM 360 computer at the Naval Postgraduate School. This particular method of spectral analysis involves the determination of the auto-covariance function, which is first smoothed, and then the power spectrum is computed through Fourier transformation. The auto-covariance function of the wave record time series, $X_1(t)$ is expressed as the average lagged product, and is defined as,

$$\phi_{11}(\tau) = \lim_{T\to\infty} \frac{1}{T} \int_{-T/2}^{T/2} X_1(t)\, X_1(t+\tau)\, dt \tag{3.6}$$

where τ = time lag.

Due to the finite nature of the given continuous record, the auto-covariance function is expressed within set limits for all values of τ.

This finite expression is called the apparent auto-covariance function and is written as,

$$\phi_{\infty}(\tau) = \frac{1}{T_n - |\tau|} \int_{-(T_n - |\tau|)/2}^{(T_n - |\tau|)/2} X_1(t)\, X_1(t+\tau)\, dt \quad (3.7)$$

where T_n = the length of the record.

A filtering function, called a lag window, is introduced to restore the features of the true spectrum. A Parzen lag window is used here and is defined as,

$$D_p(\tau) = 1 - \left(\frac{6k}{m^2}\right)\left(1 - \frac{k}{m}\right),\ k = 0,1,2\cdots\frac{m}{2} \quad (3.8)$$

where m = the total number of lags.

The Parzen window function is always positive, i.e., it has no negative side lobes. This window is particularly useful in calculating cross-spectra as it tends to eliminate any numerical instability problems that may arise in the analysis procedure. The modified, apparent auto-covariance function, $\phi_p(\tau)$, is then given as,

$$\phi_p(\tau) = D_p(\tau)\ \phi_{\infty}(\tau) \quad (3.9)$$

The smoothed spectral estimates are determined by taking the cosine transform of the modified, apparent auto-covariance function. This final representation is called the power spectrum and is expressed as,

$$\Phi_{11}(\sigma) = \frac{1}{2\pi} \int_{-\infty}^{\infty} \phi_p(\tau) \cos \sigma\tau d\tau \quad (3.10)$$

D. COMPUTATION OF CROSS SPECTRUM

For the problem at hand the cross spectra of pairs of stationary, random times series contain two different but related and extremely useful forms of information: the phase spectrum and the coherence

spectrum. The phase spectrum measures the phase difference between the two processes, and the coherence spectrum is a measure of the correlation between the two processes, at each spectral frequency band.

By definition, the cross spectrum, Φ_{12}, is the Fourier transform of the cross-covariance function with both odd and even functions of their respective arguments, and can be written as,

$$\Phi_{12}(\sigma) = \frac{1}{2\pi} \int_{-\infty}^{\infty} \phi_{12}(\tau)(\cos \sigma\tau - i \sin \sigma\tau)\, d\tau \qquad (3.11)$$

where X_1 = the wave record time-series for sensor No. 1.

X_2 = the wave record time-series for sensor No. 2.

ϕ_{12} = the cross-covariance function between X_1 and X_2 given by,

$$\phi_{12}(\tau) = \lim_{T\to\infty} \int_{-T/2}^{T/2} X_1(t)\, X_2(t+\tau)\, dt \qquad (3.12)$$

In the actual computer analysis, the cross-covariance function is modified by the Parzen lag window, but for simplicity in terminology, the apparent, modified cross-covariance function will be referred to as the cross-covariance function.

The cross spectrum as a complex-valued function of σ can be written as

$$\Phi_{12}(\tau) = \frac{1}{2\pi} \left\{ \int_{-\infty}^{\infty} \phi_{12}(\tau) \cos \sigma\tau d\tau - i \int_{-\infty}^{\infty} \phi_{12}(\tau) \sin \sigma\tau d\tau \right\} \qquad (3.13)$$

This spectral function combines both the cosine and sine transforms of $\phi_{12}(\tau)$ and can be resolved into odd and even complements. Since the cosine (sine) transforms of an odd (even) function is zero, the cross spectrum can then be expressed in this simplified form,

$$\Phi_{12}(\sigma) = \frac{1}{2\pi}\left\{\int_{-\infty}^{\infty} \phi_{even}(\tau)\cos\sigma\tau d\tau - i\int_{-\infty}^{\infty} \phi_{odd}(\tau)\sin\sigma\tau d\tau\right\} \quad (3.14)$$

A useful property of the cross-covariance function which will be used extensively later in the analysis can be shown by replacing τ by $-\tau$, and then making the substitution $\delta = t-\tau$ to obtain,

$$\phi_{12}(-\tau) = \lim_{T\to\infty} \int_{-T/2}^{T/2} X_1(\delta+t)\, X_2(\delta)d\delta \quad (3.15)$$

Since the variable of integration here is a dummy variable, a valid expression of the cross-covariance as an even function is,

$$\phi_{12}(-\tau) = \phi_{21}(\tau) \quad (3.16)$$

At this stage of the analysis, useful functions $A_{12}(\tau)$ and $B_{12}(\tau)$ are defined by,

$$A_{12}(\tau) = \frac{\phi_{12}(\tau) + \phi_{21}(\tau)}{2}$$
$$B_{12}(\tau) = \frac{\phi_{12}(\tau) - \phi_{21}(\tau)}{2} \quad (3.17)$$

Replacing τ by $-\tau$ in each expression and making use of the relationships of (3.16) yields the expressions,

$$A_{12}(-\tau) = A_{12}(\tau), \text{ and}$$
$$B_{12}(-\tau) = -B_{12}(\tau) \quad (3.18)$$

where $A_{12}(\tau)$ is an even function and $B_{12}(\tau)$ is an odd function.

Since, by algebraic manipulation, $\phi_{12}(\tau)$ can be resolved as,

$$\phi_{12}(\tau) = A_{12}(\tau) + B_{12}(\tau) \quad (3.19)$$

the functions $A_{12}(\tau)$ and $B_{12}(\tau)$ are, respectively, the desired even and odd parts of the cross-covariance function. Expression (3.14) can now be written as,

$$\Phi_{12}(\sigma) = \frac{1}{2\pi}\left\{ \int_{-\infty}^{\infty} A_{12}(\tau) \cos \sigma\tau d\tau - i \int_{-\infty}^{\infty} B_{12}(\tau) \sin \sigma\tau d\tau \right\} \qquad (3.20)$$

The real part in the above expression defines the co-spectrum, $C_{12}(\sigma)$, and the negative of the imaginary part defines the quadrature spectrum, $Q_{12}(\sigma)$. The cross spectrum is then written in simplified complex form as,

$$\Phi_{12}(\sigma) = C_{12}(\sigma) - i\, Q_{12}(\sigma) \qquad (3.21)$$

It should be noted at this stage of the analysis that the co-spectrum is the cosine transform of the even part of the cross-covariance function. Analogously, the cosine transform of the auto-spectrum is the power spectrum of the record. The power spectrum is defined as showing the contribution to the total variance of a single record in the indicated bands of frequency, and has the same significance as the even part of the cross-covariance function; the evenness expresses the cross-covariance of the in-phase (zero degree) components or reversed phase ($\pm$ 180 degrees) components between the two records.

The quadrature spectrum, with a similar argument, can be shown to represent the amount of power due to components which are out of phase by a constant amount ($\pm$ 90 degrees).

The spectral phase difference, $\varepsilon_{12}(\sigma)$, is defined as the argument of the complex conjugate of the cross spectrum and is written as,

$$\varepsilon_{12}(\sigma) = \tan^{-1} \frac{Q_{12}(\sigma)}{C_{12}(\sigma)} \qquad (3.22)$$

The spectral phase difference represents the average phase angle by which the cross-correlated components of X_1 lead those of X_2 in each spectral frequency band.

The coherence is extremely important as a meaningful estimator of the creditability of the phase spectra in each spectral frequency band. Not all the frequency components from the two synchronized random records may be cross-correlated, contrasted with the perfect correlation (at zero lag) of the components of the individual power spectra. This comparison can be exhibited by a ratio of the cross spectrum to the square root of the individual auto-spectra and is written as,

$$R(\sigma) = \frac{|\Phi_{12}(\sigma)|}{\left[\Phi_{11}(\sigma)\ \Phi_{22}(\sigma)\right]^{1/2}}$$

This coherency function can then be expressed quite simply as,

$$R(\sigma) = \left[\frac{C_{12}^2(\sigma) + Q^2(\sigma)}{\Phi_{11}(\sigma)\ \Phi_{22}(\sigma)}\right]^{1/2} \leq 1$$

This ratio plays the role of a correlation coefficient defined for each spectral frequency band.

IV. INSTRUMENTATION

A. SENSOR LOCATION

The wave data obtained were recorded from three wave sensors placed in a line normal to the breakwater (Figure 4). The distance between the two seaward sensors was pre-planned at 135 feet, which is one-quarter wave length of a 14-second wave in 46 feet of water. This period coincides with the most frequently occurring wave period for the months of November to January, which is approximately 14 seconds as determined from sea and swell data for incident waves in the vicinity of the harbor [Wilson, Hendrickson, and Kilmer, 1965]. The actual seaward sensor separation was determined by transit and range lines to be 130 feet. The seaward sensors (No. 1 and No. 2) are at depths of 45 and 47 feet, for an average depth of 46 feet (MLLW). The locations of the sensors with respect to the breakwater can be seen in Figures 9 and 10.

Although not imperative in the analysis of the partial standing wave phenomenon, the separation between sensor No. 2 and the breakwater face at MLLW was established at 135 feet in an effort to observe the standing wave under ideal conditions. Sensor No. 2 was approximately 135 feet from the breakwater face at MLLW, and approximately 100 feet horizontally from the base of the breakwater. This separation is considered necessary for wave records to be uneffected by the turbulence of the wave upwash or other related effects at the face of the breakwater. The horizontal separation between sensor No. 3 (harbor) and the breakwater face at MLLW is approximately 80 feet which is necessary for a balance between minimum diffraction and negligible turbulence effects. Location of the harbor sensor is such that diffraction may be considered negligible.

FIGURE 9

Seaward Sensor Positions

FIGURE 10

Harbor Sensor Position

B. SEAWARD SENSORS

The two sensors used to seaward of the breakwater are identical Marine Advisors Model A-2b instruments modified from the basic Frank E. Snodgrass Mark IX design. The A-2b sensor consists of two oil-filled chambers connected through a capillary tube and, in a parallel flow path, a strain-gauge differential pressure transducer. One chamber is exposed to sea pressure with fluid separation accomplished by a neoprene diaphragm. The second chamber serves to introduce compliance into the system by means of a spring-loaded, air filled bellows which allows flow through the capillary to slowly equalize the pressure between the chambers. Rapid pressure fluctuations, such as those due to wind-driven waves and swell, result in an insignificant amount of flow through the capillary, and a pressure differential is registered between the chambers. Slow variations in pressure, such as those due to tides and seiches, cause sufficient flow during intervals of time much shorter than their period to prevent a significant pressure differential from being maintained across the transducer. When in this configuration, the device becomes a hydraulic analog of an electrical RC high-pass filter circuit. The two A-2b sensors are hydraulically filtered at time constants of 47 and 50 seconds and produce a uniform flat response curve for sea and swell data.

When placed on the sea floor, the A-2b transducer senses the pressure signature of the waves present in the form of short-period deviations from the average pressure at the instrument. The interpretation of the pressure fluctuations is modified by a hydrodynamic attenuation factor that is a function of the depth at the instrument, elevation of the instrument above the bottom, and the period of the

waves being observed. The sensors are tripod mounted (Figure 11). The seabed in the vicinity of the seaward sensors is a relatively flat, clay surface with bottom contours generally straight and parallel to the breakwater. These bottom characteristics result in negligible shoaling and refraction in the vicinity of the seaward wave sensors.

C. HARBOR SENSOR

The single sensor used on the harbor side of the breakwater is a Frank E. Snodgrass Mark IX design. The sensor's principle component is a Bourns differential pressure potentiometer which is used as the transducer. Hydraulic filtering at a time constant of 60 seconds, comparable in theory and sensitivity to the Marine Advisors A-2b sensors, is achieved in the Mark IX model. The harbor sensor is in an approximate depth of 39 feet at mean lower low water. Linearity and resolution of $\pm$ 1 per cent of full-scale deflection is obtained through sensitivity control adjustment of the instrument. This provides a uniform flat response curve for sea and swell data.

D. WAVE RECORDERS

The seaward wave data obtained using the Marine Advisors A-2b sensors were recorded by a solid-state, modular-construction, Clevite Brush recorder. Wave data from both sensors were recorded simultaneously with two single-channel, plug-in modules on pressure-sensitive paper with a rectilinear trace presentation. This multi-trace design insures the accurate synchronization between both sensors required for cross spectra calculations. The chart speed used was 0.4 millimeter per second.

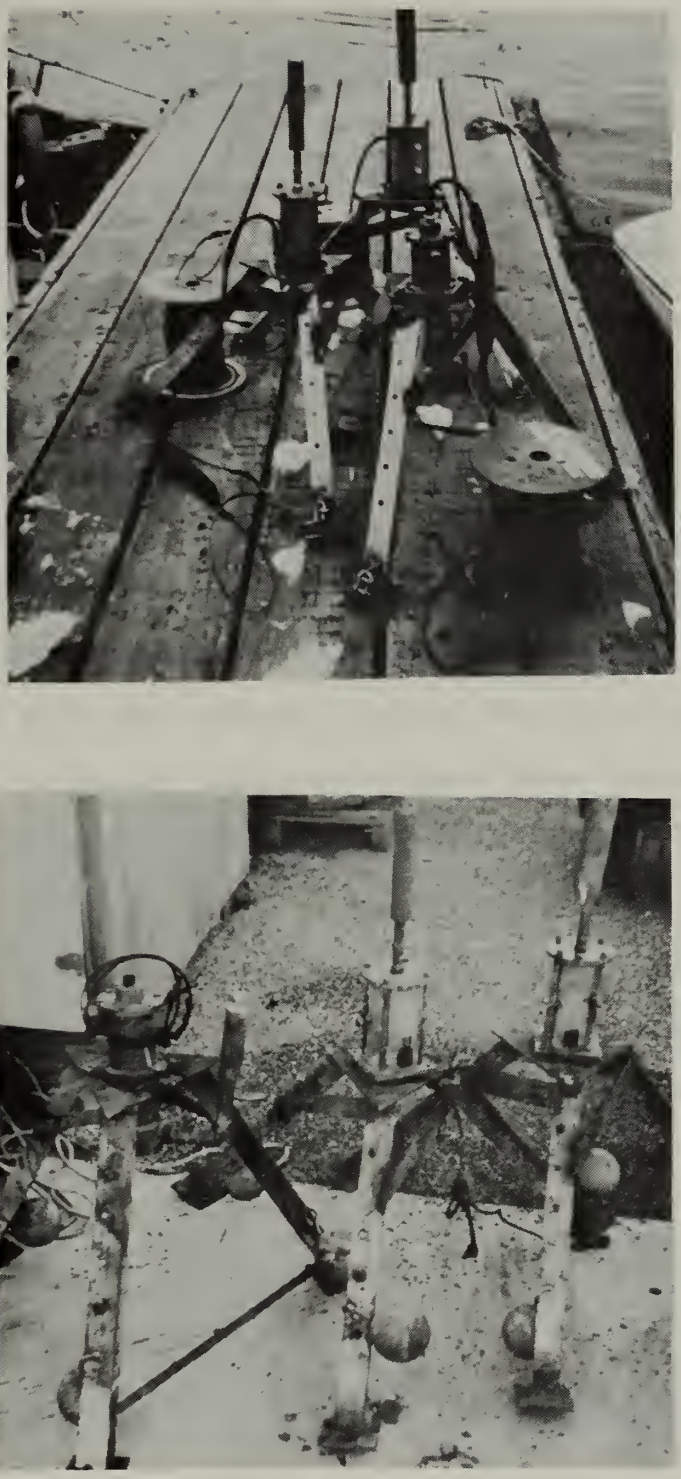

FIGURE 11

Wave Sensor Mounts
Before Study (above) and After Study (below)

Manufacturer's claims for the Brush Recorder are that hysteresis is limited to ± 1 per cent of the full-scale value. Individual channel modules were calibrated with their respective sensors and associated equipment before final placement. Calibration figures were prepared at five volts excitation using a plus and minus five-foot dynamic head pressure fluctuation achieved by lowering and raising the sensors in a sea-water tank. After numerous trials, a linear variation of ± 1-1/2 per cent from best straight line was realized for each transducer.

The harbor data obtained using the Snodgrass Mark IX sensor was recorded on an Esterline-Angus model AW strip-chart recorder. Attached power supply and bridge circuit components were part of the general purpose Mark IX shore wave recorder system. Wave data were recorded from sensor No. 3 (harbor) with a curvilinear trace presentation. The chart speed utilized was 3/4 inch per minute (0.29 millimeter per second).

Calibration circuitry unique to the Mark IX shore wave recorder is incorporated as a functional component of the system. Calibration checks were routinely taken and adjustments were made for deviations from set current values for full-scale deflection.

V. ANALYSIS OF RESULTS

A. INTERPRETATION OF POWER SPECTRA

1. Measured Power Spectra

A power spectrum of a stationary random process is considered to be the statistical estimate of the energy according to frequency bands obtained through integration of the spectral density. This spectral representation is the Fourier transform of the auto-covariance function. This concept of spectral analysis is based on an assumption that the energy contained in wind waves and swell can be represented through linear theory by the sum of the energy contained in many individual wave trains. Therefore, the total area under the spectral density curve will be proportional to the total energy.

The power spectra traces for the three sensors for six sets of wave measurements are plotted in Figures 12, 16, 20, 24, 28 and 32. The individual traces for all three sensors are superimposed over the same frequency interval scale, but the scale of the spectral density ordinate for the seaward sensors (No. 1 and No. 2) and the harbor sensor (No. 3) is ten to one, respectively. The power spectrum for each sensor was computed from time records digitized at 0.63 second intervals giving a Nyquist frequency of 1.26 seconds, a resolution of 0.00389 Hz, and a total effective record length of 21.5 minutes. Due to the increasingly significant hydrodynamic attenuation factors with increasing frequency (e.g., 0.40 at 0.15 Hz), the high frequency range of the spectral plots was limited to 0.15 Hz (6.7 sec).

Sensors No. 1, No. 2, and No. 3 were hydraulically high-pass filtered at time constants of 47, 50, and 60 seconds, respectively. This

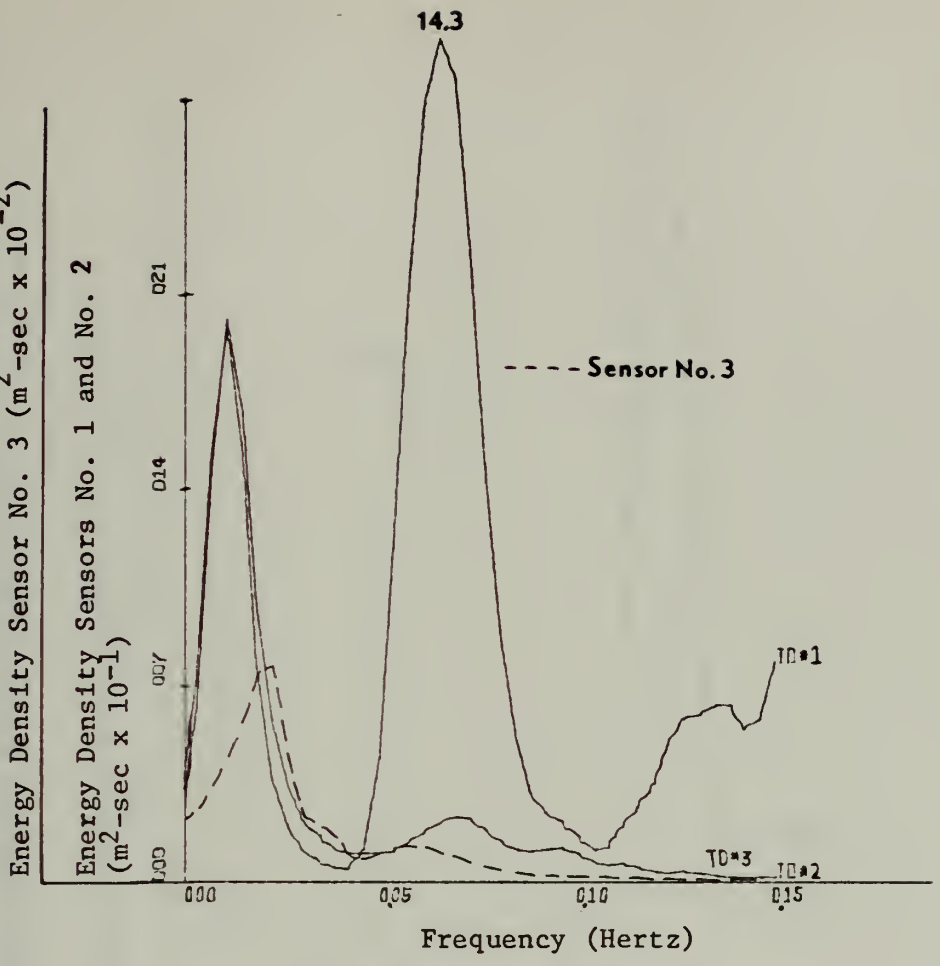

FIGURE 12

Measured Power Spectra, High Tide, 17 Dec 70 (1330)

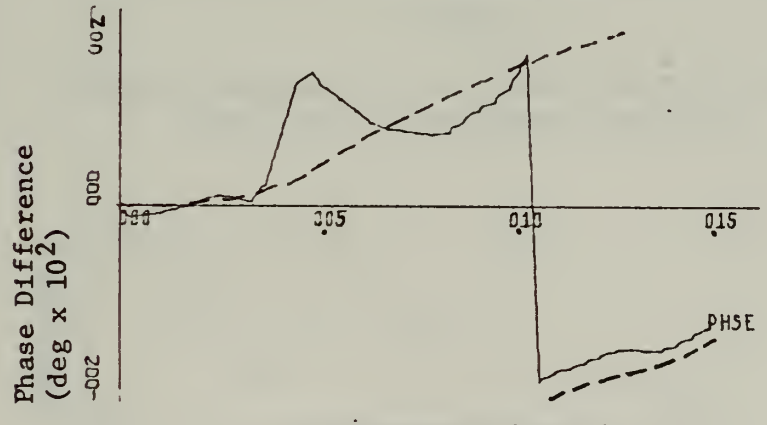

FIGURE 13

Phase Spectrum, High Tide, 17 Dec 70 (1330)

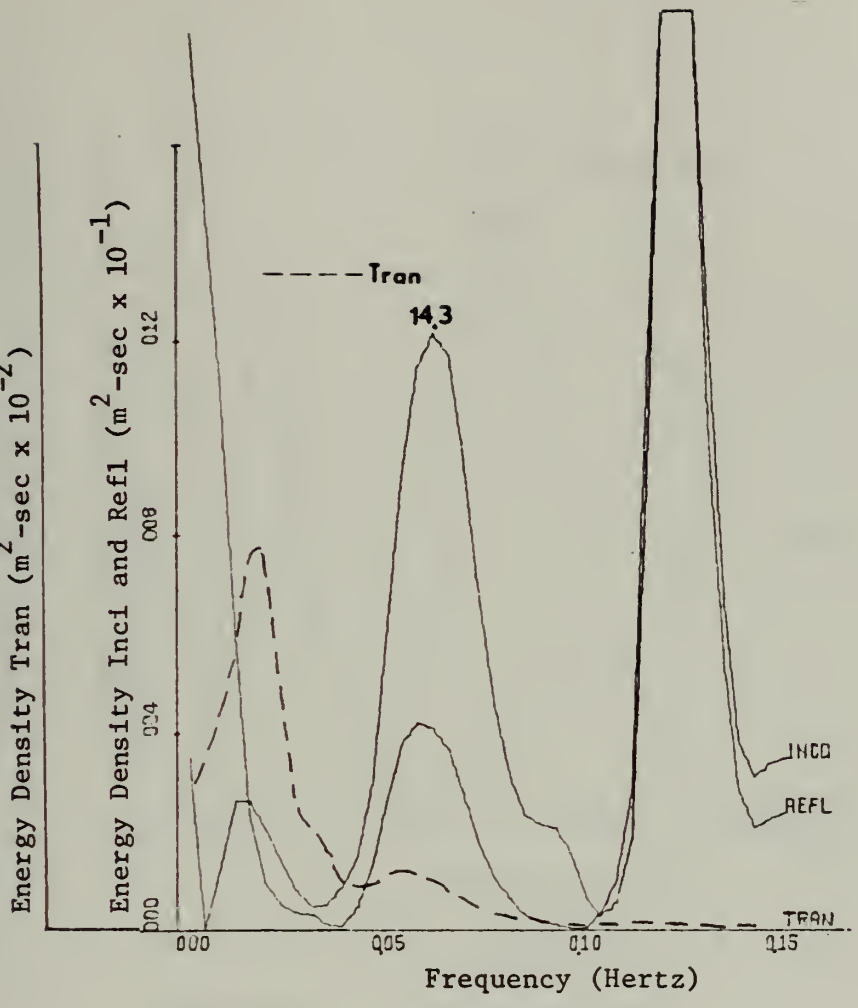

FIGURE 14

Incident, Reflected, and Transmitted Power Spectra
High Tide, 17 December 1970 (1330)

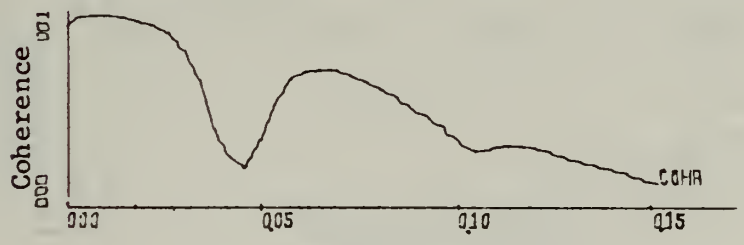

FIGURE 15

Coherence Spectrum, High Tide, 17 December 1970 (1330)

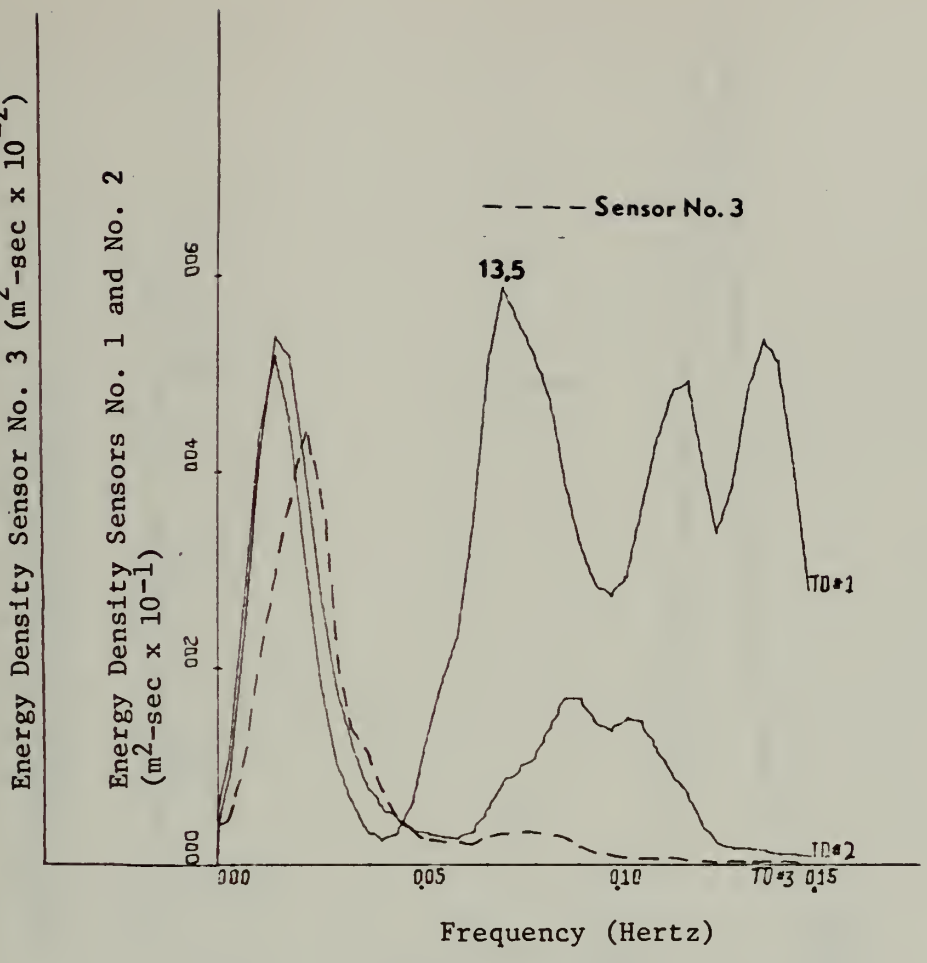

FIGURE 16

Measured Power Spectra, High Tide, 1 Dec 70 (0800)

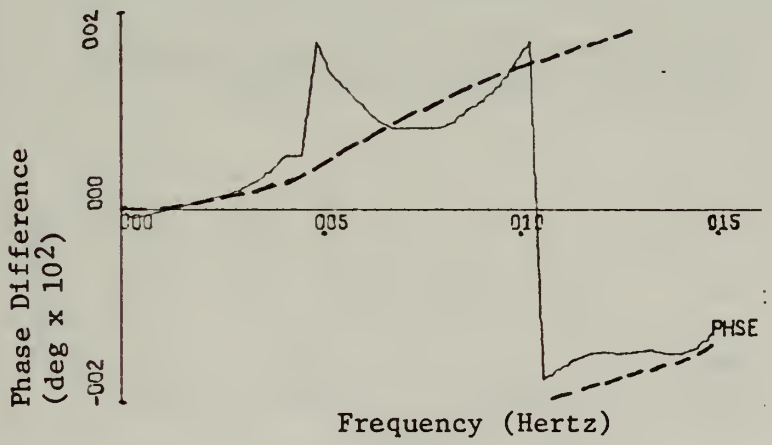

FIGURE 17

Phase Spectrum, High Tide, 1 Dec 70 (0800)

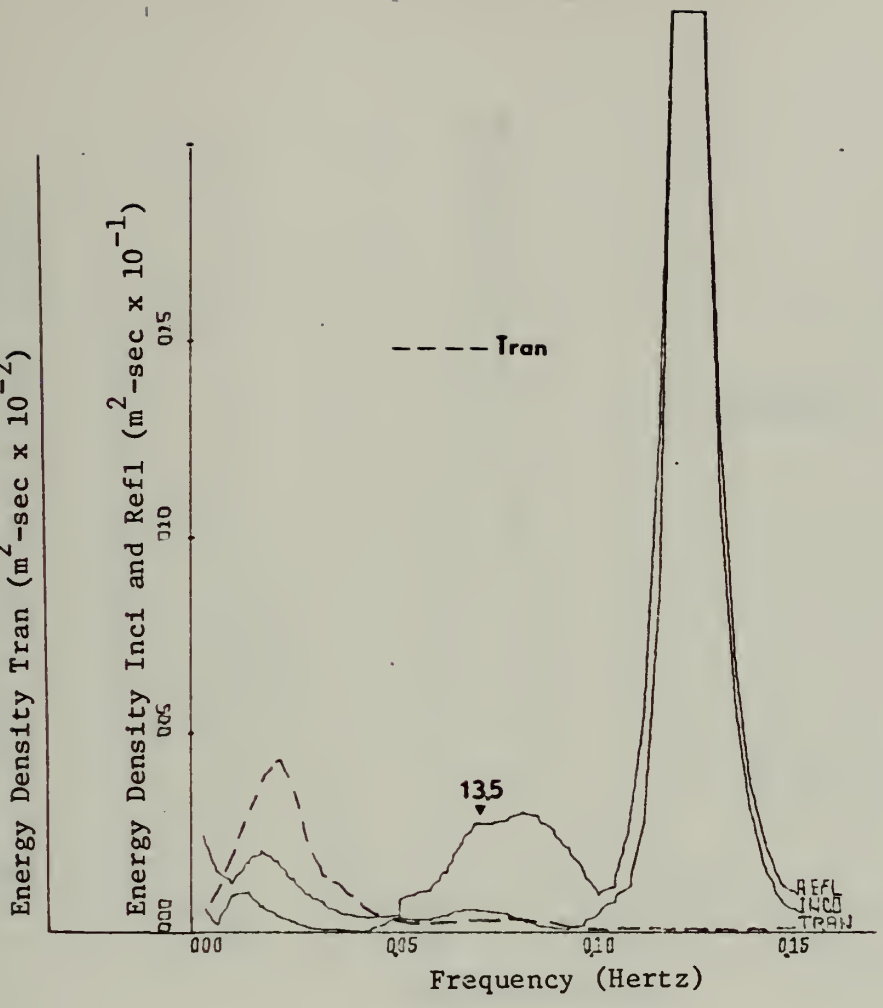

FIGURE 18

Incident, Reflected, and Transmitted Power Spectra
High Tide, 1 December 1970 (0800)

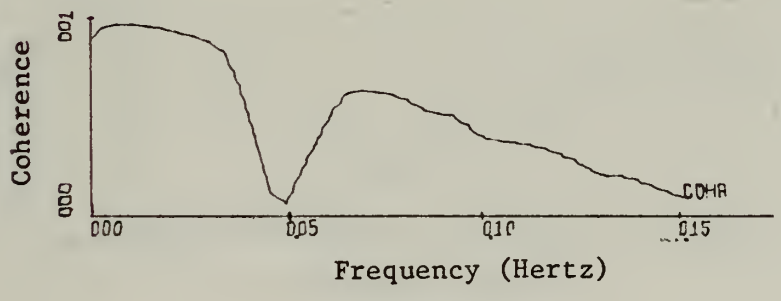

FIGURE 19

Coherence Spectrum, High Tide, 1 December 1970 (0800)

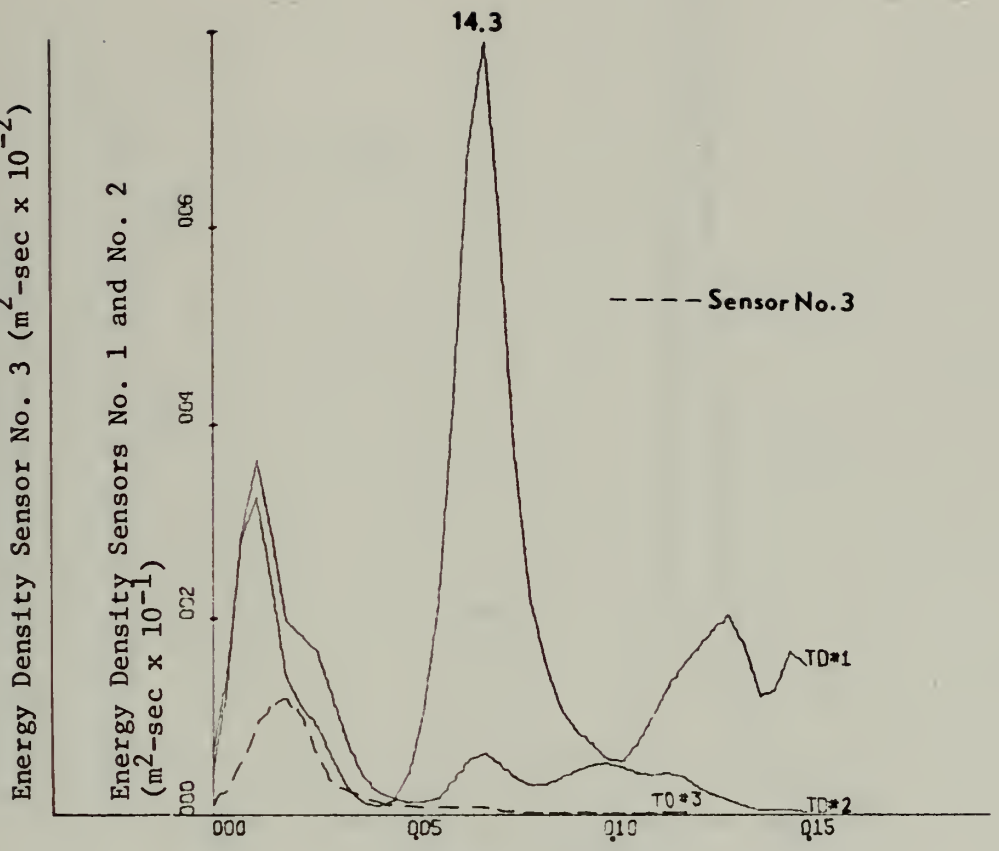

FIGURE 20

Measured Power Spectra, Low Tide, 1 Dec 70 (2000)

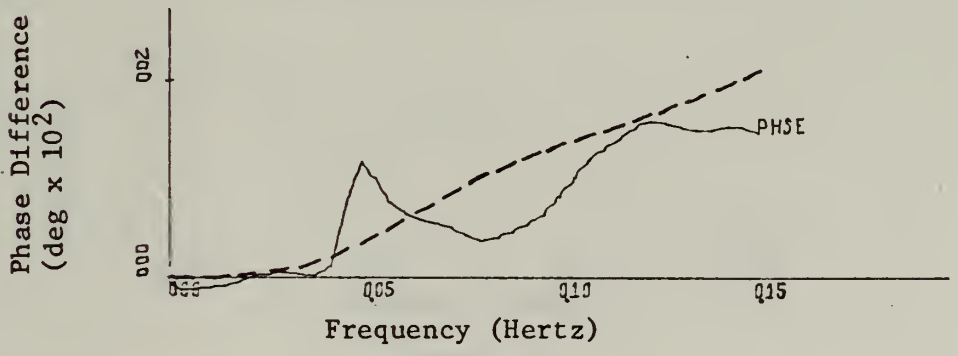

FIGURE 21

Phase Spectrum, Low Tide, 1 Dec 70 (2000)

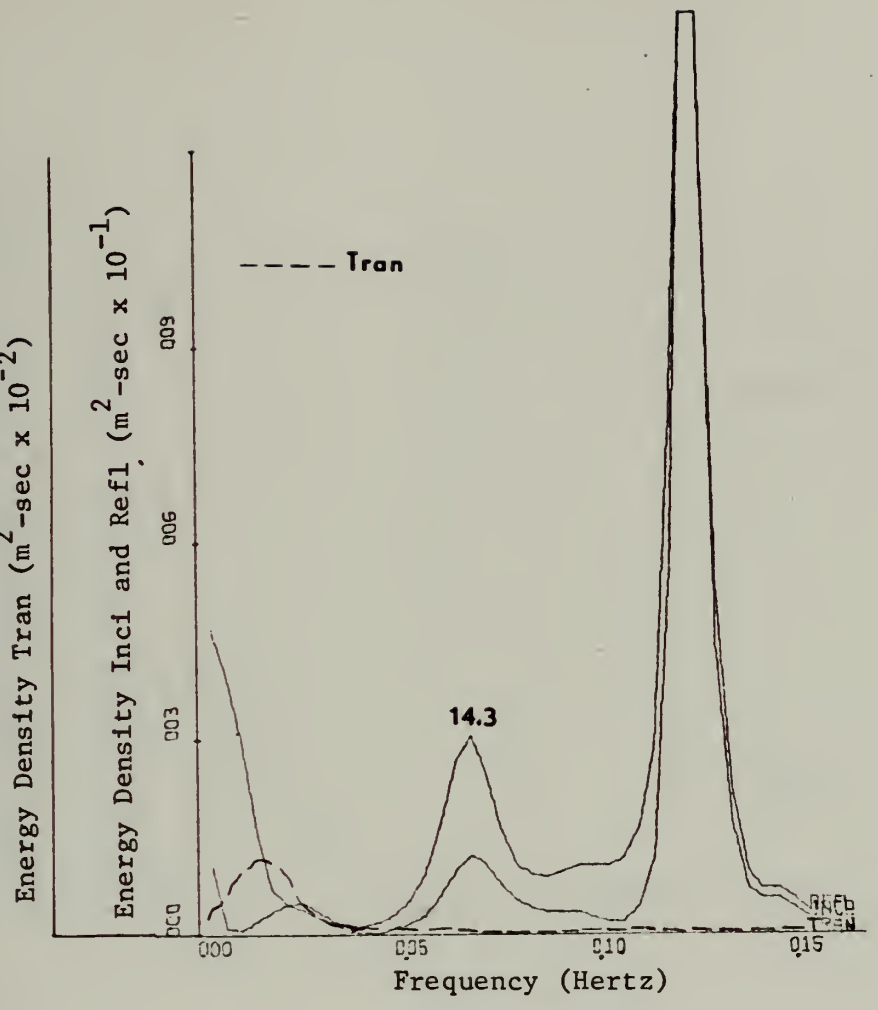

FIGURE 22

Incident, Reflected, and Transmitted Power Spectra
Low Tide, 1 December 1970 (2000)

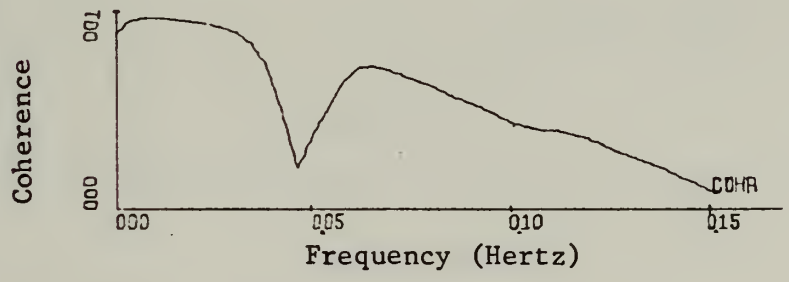

FIGURE 23

Coherence Spectrum, Low Tide, 1 December 1970 (2000)

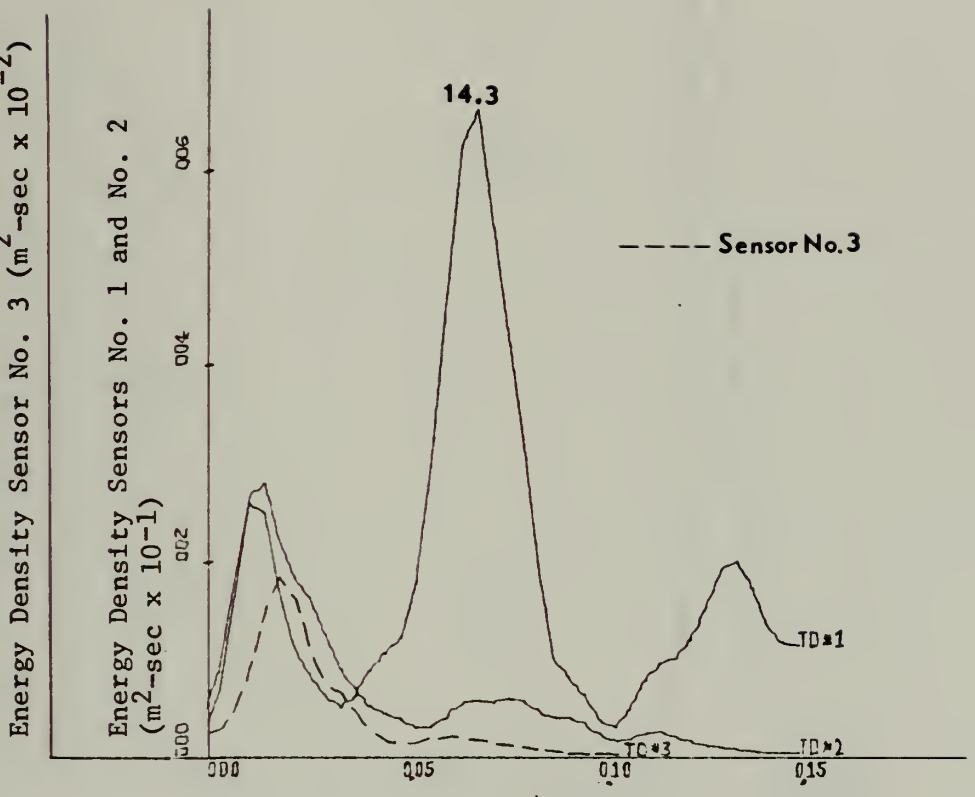

FIGURE 24

Measured Power Spectra, Low Tide, 1 Dec 70 (2330)

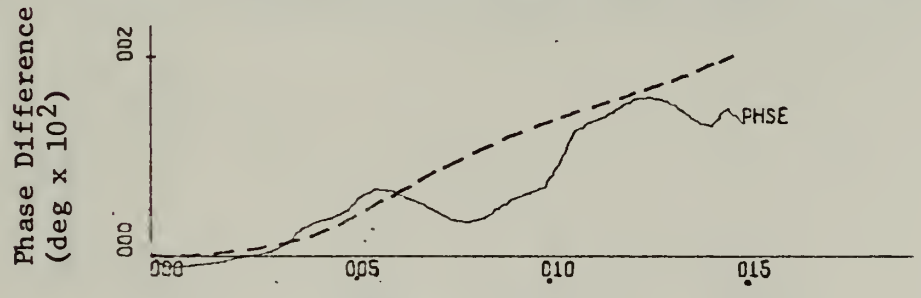

FIGURE 25

Phase Spectrum, Low Tide, 1 Dec 70 (2330)

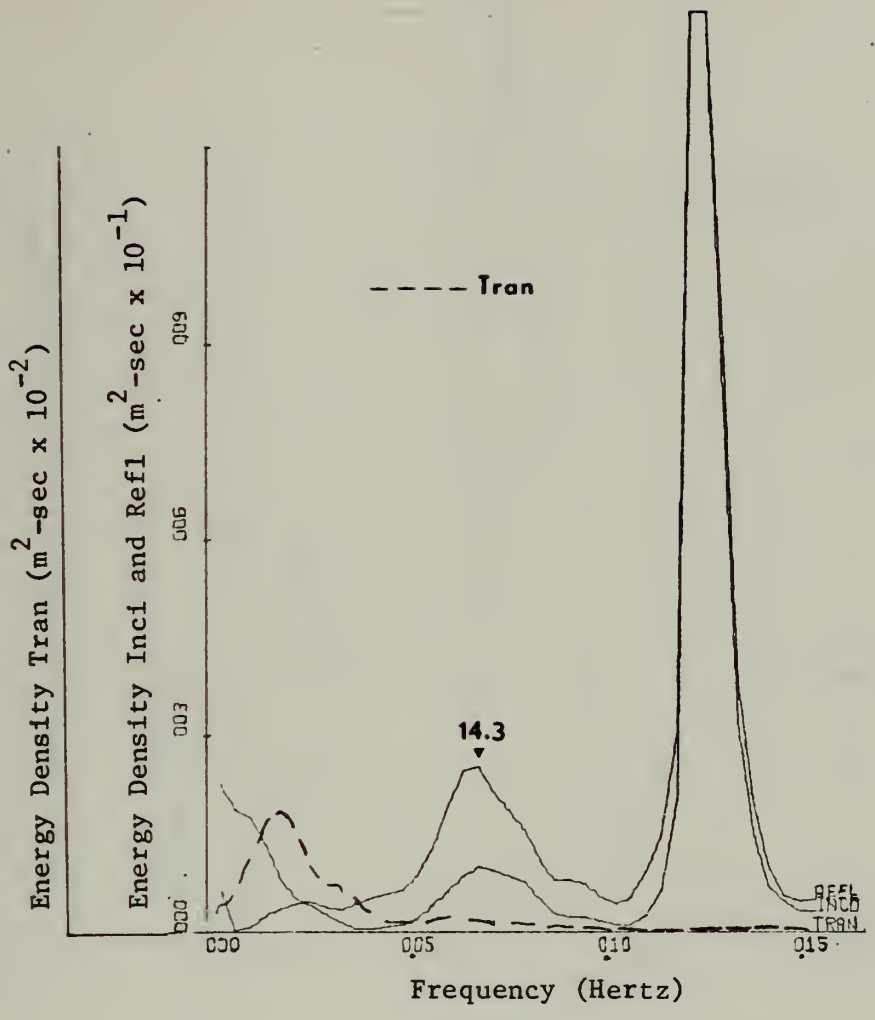

FIGURE 26

Incident, Reflected, and Transmitted Power Spectra
Low Tide, 1 December 1970 (2330)

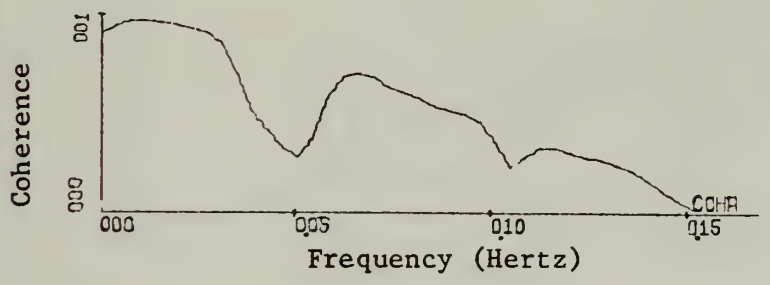

FIGURE 27

Coherence Spectrum, Low Tide, 1 December 1970 (2330)

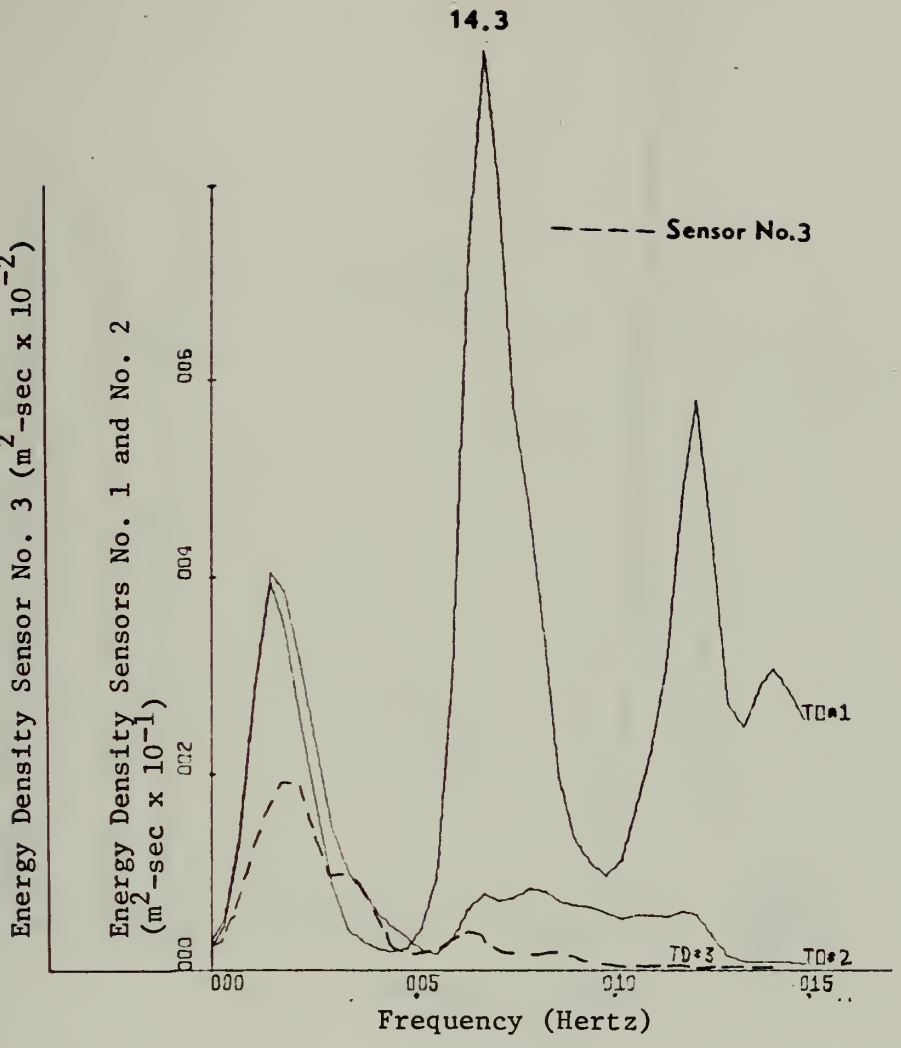

FIGURE 28

Measured Power Spectra, Low Tide, 2 Dec 70 (2030)

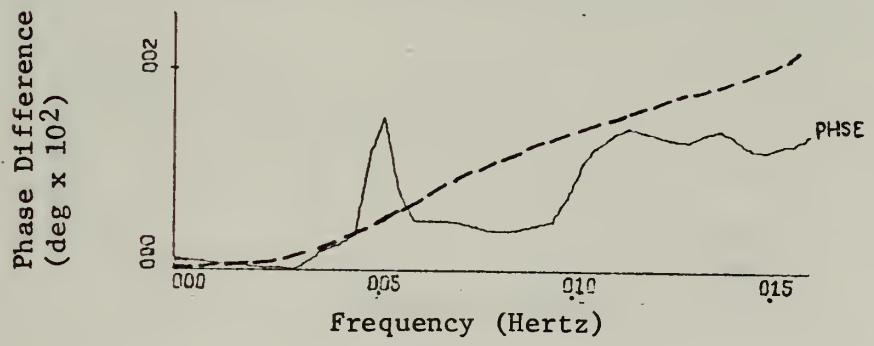

FIGURE 29

Phase Spectrum, Low Tide, 2 Dec 70 (2030)

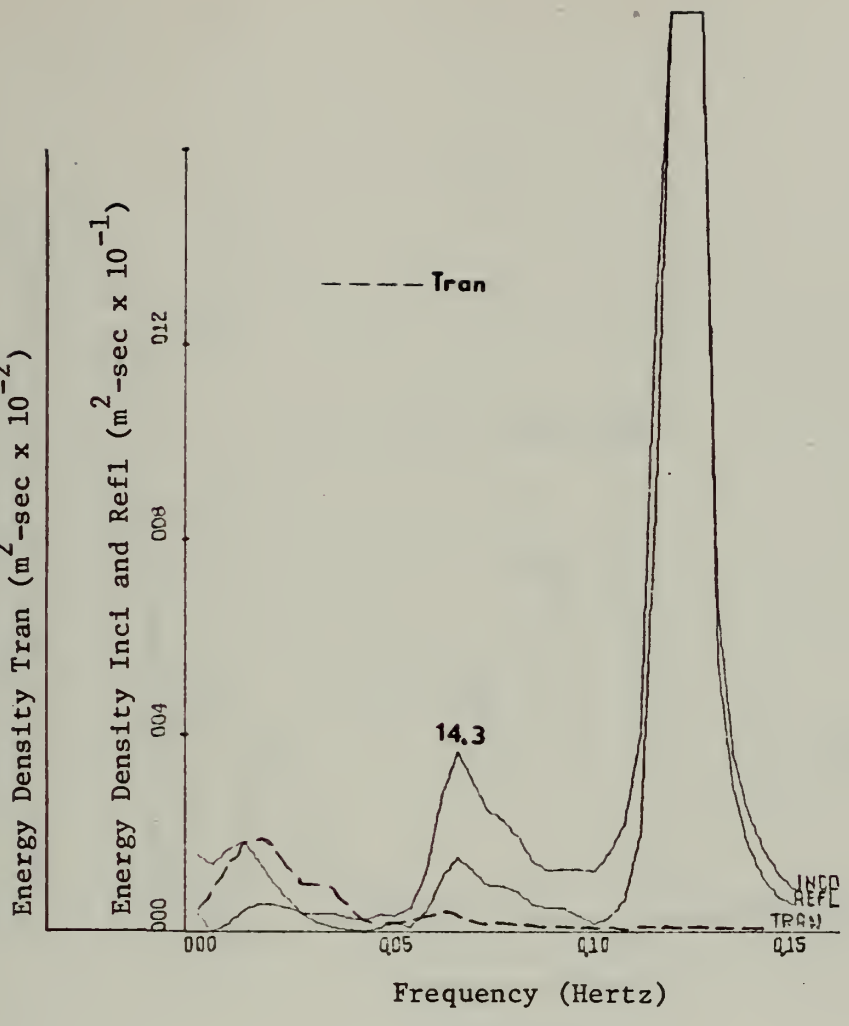

FIGURE 30

Incident, Reflected, and Transmitted Power Spectra
Low Tide, 2 December 1970 (2030)

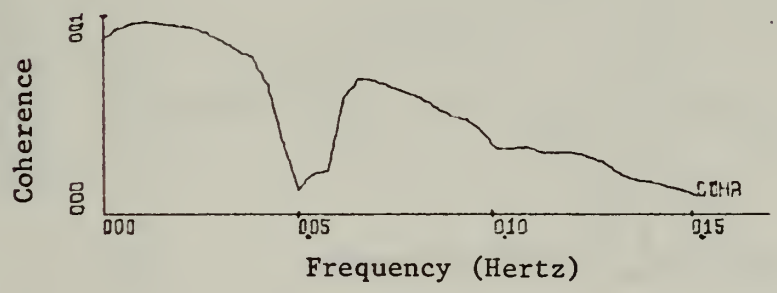

FIGURE 31

Coherence Spectrum, Low Tide, 2 December 1970 (2030)

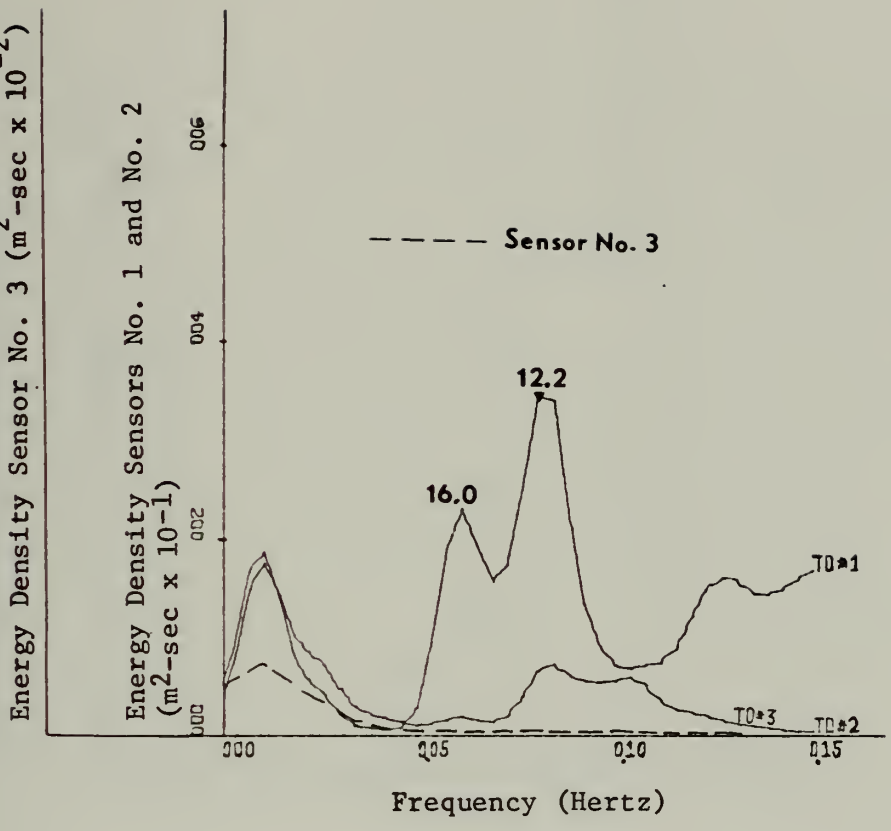

FIGURE 32

Measured Power Spectra, Low Tide, 14 Dec 70 (1600)

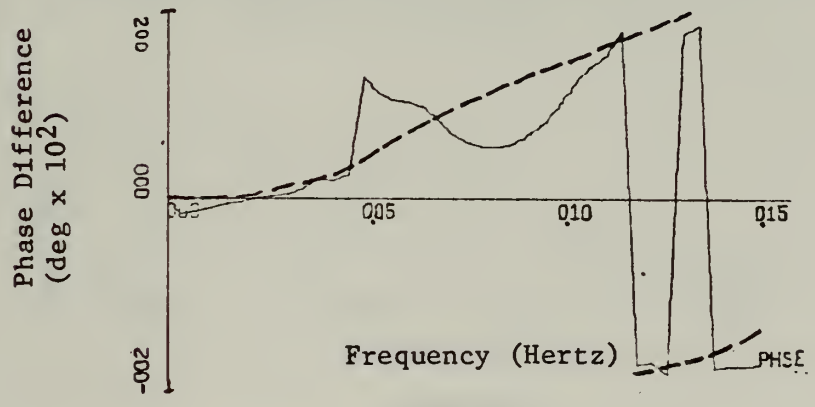

FIGURE 33

Phase Spectrum, Low Tide, 14 Dec 70 (1600)

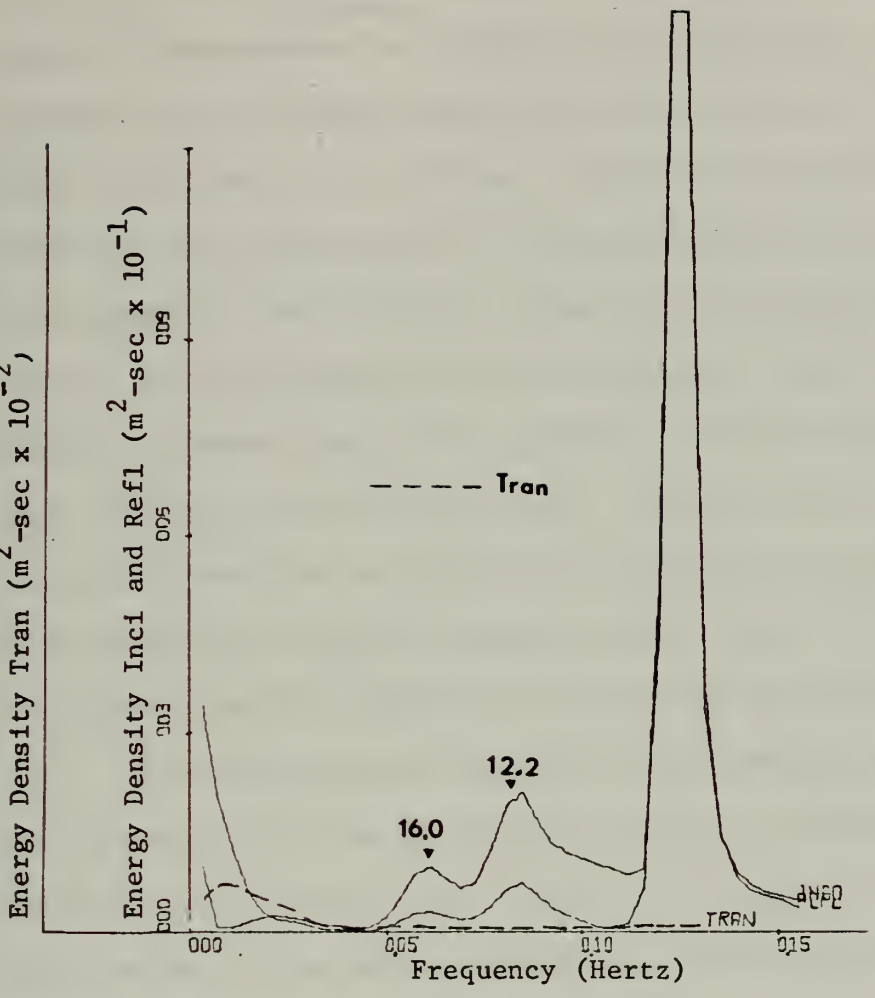

FIGURE 34

Incident, Reflected, and Transmitted Power Spectra
Low Tide, 14 December 1970 (1600)

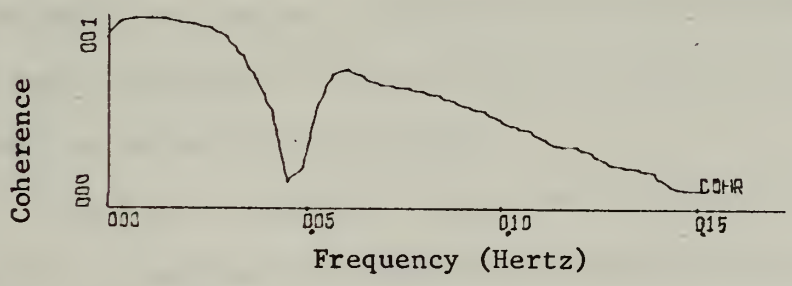

FIGURE 35

Coherence Spectrum, Low Tide, 14 December 1970 (1600)

caused substantial dampening (filtering) at an exponentially increasing rate for spectral components below the frequencies corresponding to the respective time constants. Taking the dampening into consideration, tangible spectral energy density was still evident at the lower frequencies dealt with below 0.02 Hz (50 sec). These low frequency, filtered, spectral densities have been included in the power spectrum plots for information with regard to their relative, rather than absolute, spectral density values. Of particular note is the strikingly similar energy density spectra of seaward sensors No. 1 and No. 2 (both similarly damped) in this long wave, low frequency range. Considering the relatively short distance between the two sensors and the long wave lengths for the spectral wave components within this range of nearly equal spectral densities, it is apparent that the instrument calibrations are consistent and accurate.

All of the spectra analyzed reveal prominant peaks within the period range from 50 to 60 seconds; sensor No. 3 (harbor) in the vicinity of 50 seconds and sensors No. 1 and No. 2 (seaward) nearer 60 seconds. Confirmation of the spectral prominances for these sensors in the 50 to 60 seconds range was also found in earlier studies. In particular, Hudson [1949] indicates persistent spectral peaks at 55 seconds in Monterey Harbor. Wilson, Hendrikson, and Kilmer [1965] found through the technique of residuation analysis of long-wave records that spectral peaks occur frequently at both 60 and 45 seconds for waves within and incident at the mouth of the harbor.

There is a remarkably high, narrow-banded spectral peak for sensor No. 1 centered at a frequency corresponding approximately to a 14-second period in all the wave records analyzed. This persistent feature is particularly interesting in that it coincides with the

theoretical anti-nodal line prediction of maximum wave amplitude for the prearranged sensor location (a 14-second period quarter wave length separation between sensor No. 1 and No. 2, and sensor No. 2 and the breakwater face at MLLW). Correspondingly, a relatively small and flat energy density spectrum at sensor No. 2 is found which is located at the theoretical nodal position for a 14-second period wave. Spectrum analysis thus provides confirmation that a fairly well-defined partial standing wave phenomenon exists to seaward of the reflecting breakwater. Standing waves were at times observed distinctly in the wave records when a well defined 14-second period sinusoidal swell was recorded at sensor No. 1, while at the same time a relatively flat nodal area was observed at sensor No. 2 (Figure 36).

In all six wave recordings, sensor No. 1 shows appreciable energy in the special frequency range of interest, 0.11 to 0.044 Hz (9 to 23 sec), whereas, sensor No. 2 shows considerably less energy but does have parallel persistency in spectral peaks for approximately the same frequency range. The subsidiary prominant spectral peaks that appear at frequencies above 0.11 Hz (9 sec) will be interpreted in the following section.

The power spectra for sensor No. 3 (harbor) is for the most part comparatively flat in the frequency range of special interest (0.11 to 0.044 Hz). In contrast to the high peaks and deep valleys of the seaward spectra, the harbor spectrum drops off to significantly low values above 0.11 Hz (9 sec) and has generally persistent high values below 0.044 Hz (23 sec). The spectral peak in the low frequency range closely parallels the seaward spectra in both persistence and frequency. This increase in spectral amplitudes in the lower frequencies is partially obscured due to

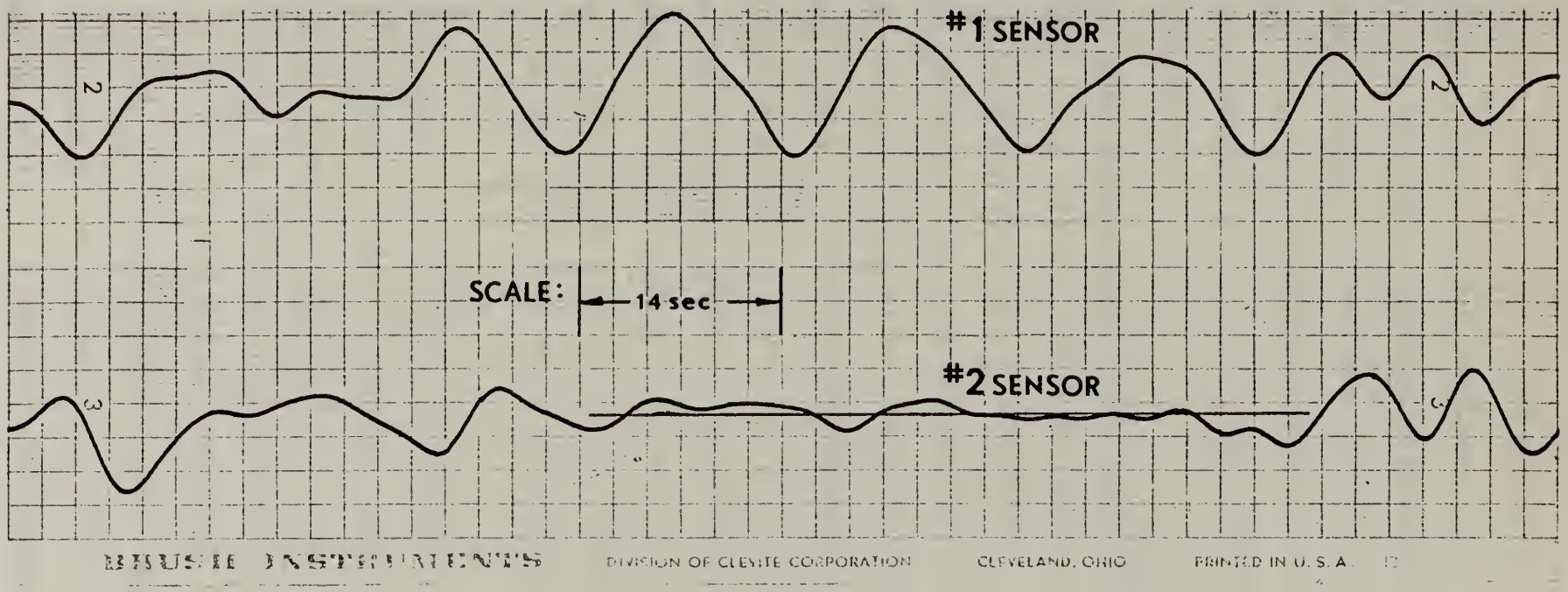

FIGURE 36

Analog Trace Illustrating Partial Standing Wave Phenomenon

the inherent hydraulic filtering (60-second time constant). Although this feature does not prove a serious hindrance for the purpose of this study, the filtering does limit quantitative interpretation of the transmitted low frequency energy. The definite increase in energy transmission toward the lower frequencies can partly be explained through the generalization that the breakwater acts as a moderately selective filter of short wave energy transmission.

2. Incident and Reflected Sea Surface Power Spectra

The incident and reflected sea surface power spectra are theoretically derived quantities already discussed in this paper under theoretical considerations. The incident and reflected spectral wave amplitudes are computed for respective spectral frequency components. From these analytically developed spectral amplitudes the power spectra were computed and are plotted in Figures 14, 18, 22, 26, 30 and 34.

The sea and swell wave energy is seen to be concentrated in the frequency range, 0.11 to 0.044 Hz (9 to 23 sec), for the incident and reflected wave components, as expected. The transmitted wave spectrum is the same as the No. 3 spectrum, and is also plotted in the above figures.

The one prominant spectral feature apparent in both the incident and reflected wave spectra which is centered at the 0.128 Hz (7.8 sec) frequency band is an artificial energy spike. This anomaly can be readily explained as the result of nodal lines occurring at both seaward sensors (No. 1 and No. 2) at approximately the same wave period. The two seaward sensors are so positioned that they theoretically measure minimum (nodal) pressure fluctuations in the vicinity of this spectral frequency band (roughly 7 to 8 seconds). The separation of the two wave sensors corresponds to a half-wave length of a 7.5 second wave period.

This unavoidable consequence caused by the partial standing wave creates the lack of discernible pressure fluctuation measurements between the two seaward sensors for this double nodal situation. The spectral densities in the vicinity of this frequency band are theoretically indeterminate, in that the measurements give an extremely high peaked, meaningless energy spike. This undesirable spectral feature limits the high frequency range of interest for this study to 0.11 Hz (9 sec). It would have been necessary to either position the sensors differently (larger interval spacing) or use three sensors seaward of the breakwater to have resolved these frequency bands.

B. INTERPRETATION OF CROSS SPECTRA

The cross spectrum is the Fourier transform of the cross-covariance function; the cross-covariance between two time-series records describes the general dependence of the values of one time-series record on the other. The cross-covariance function has essentially the same form as the auto-covariance function except that one independent time-series record, X_1, is examined (lagged) through another time-series record, X_2, rather than through itself as with the case of the auto-covariance function. The mutual dependence between the two time-series records can be quantitatively expressed through the cross spectra phase and the coherence function. The latter, being an estimator of the relative phase stability between the two cross-correlated records, is represented by a correlation coefficient from zero to one. When the coherence is near zero, the two records are said to be uncorrelated, or incoherent. The correlation, or degree of coupling between two random records, increases as the coherence approaches unity.

Coherence spectra curves for each set of wave observations are shown in Figures 15, 19, 23, 27, 31, and 35. Low coherence or non-correlation between any two random records of the phenomenon being studied can be due to any number of causes of which the more creditable are as follows:

1. Incident wave crests not parallel to the reflecting surface, thus presenting a complex, multi-peaked, incident-reflected wave surface.

2. Significant scattering of the incident wave energy vice normal reflection due to the rough angular reflecting surface of the rubble-mound breakwater (predominately high frequency reflection).

3. Coherent energy levels so low that they are lost in background noise.

Phase spectra curves for each set of wave observations are shown in Figures 13, 17, 21, 25, 29, and 33. Based on standing wave theory, for waves normally incident, the phase relationships between seaward sensors No. 1 and No. 2 should be near zero degrees for the low frequencies approaching tidal period; near 90 degrees for frequencies of waves where the separation between the seaward sensors approaches one-quarter wave length; and near 180 degrees for one-half wave length separation. This theoretical curve is described by the dashed curve superimposed on the measured phase difference curve in each figure. The comparison between theory and data is somewhat complex and will be interpreted for different ranges of the frequency spectrum.

The frequency range from zero to 0.044 Hz (23 sec) has a theoretical phase difference varying from zero to 25 degrees, increasing with increasing frequency. The phase curves compare reasonably well on all the cross spectra phase plots in this frequency range. The coherence is high (average 0.90).

In the frequency range 0.044 to 0.05 Hz (23 to 20 sec) the large discrepancy in the phase curves for the theoretical and measured phase spectra may be explained by the fact that it is a spectral region of poor coherence (average 0.20). A plausible reason for this lack of correlation is simply the absence of any energy in the frequency band (note the minor energy density in this frequency range).

The phase spectra in the frequency range from 0.05 to 0.15 Hz (20 to 6.7 sec) shows variable deviations between the theoretical and the measured curves. The cross-correlated phase data associated with high tide on 1 December and 17 December 1970 (Figures 13 and 17) compare within a maximum deviation of approximately 25 degrees. The other cross-correlated records show somewhat less correspondence. All of the records tend toward finer correspondence of the measured and theoretical phase differences with increasing frequency. Coherence drops almost linearly from moderate (average 0.70) to poor (average 0.20) in this range. For two wave records which tend toward negligible energy density in the vicinity of 0.10 Hz (10 sec) (Figures 12 and 24), there is an expected although slight dip in coherence. Reasons for the decreasing coherence tendency within this frequency range are uncertain. The most plausible reason is the tendency for increased scattering as wavelength decreases with increasing frequency. The reflecting surface area of the angular shaped armor units relative to the decreasing wave length assumes a controlling factor which probably magnifies the scattering effect (oblique incidence to the reflecting surface). Another possible explanation is oblique wave incidence of multidirectional free wave components of the same frequency but of different origin.

C. TRANSMISSION, REFLECTION, AND ENERGY DISSIPATION COEFFICIENTS

Transmission, reflection, and energy dissipation coefficients are dimensionless parameters which describe the usefulness of a permeable breakwater. Transmission and reflection coefficients computed from the six selected time-series records (Table I) are presented according to respective spectral frequency bands in Figures 37 and 41, and the energy dissipation coefficients are presented in Figures 38 and 42. For all measurements, winds were nominal and the direction of sea and swell was visually observed to be within ten degrees of normal incidence to the breakwater. Data scatter is significant only at the high and low boundaries of the spectral frequency range of interest, 0.11 and 0.044 Hz (9 and 23 sec). The reasons for the scatter are directly related to the previous discussion of power and cross spectra pertaining to the anomalous measurements in these select border frequency bands.

Figures 37 and 38 describe the coefficients at high tide conditions (average four feet MLLW) for two time-series records (Table I). Both wave records were at incipient wave overtopping of the breakwater (Figures 39 and 40). The coefficient of transmission has a nearly uniform value of about 0.10 from 0.11 to 0.067 Hz (9 to 15 sec), below which increases almost exponentially as frequency decreases. This increase can be aptly explained as the result of the longer wave length of the incident lower frequency wave components.

The wave reflection coefficient decreases almost linearly with increasing frequency due to the progressively dominating influences of the scattering of the incident wave energy as the wave length decreases. The energy dissipation coefficient, which is primarily due to the random scattering, turbulence, and the internal frictional resistance of the

TABLE I

Monterey Breakwater Wave Data from Field Study

DATE	TIDE STATE (TIME)	PERIOD OF PEAK ENERGY CONCENTRATION (sec)	SIGNIFICANT WAVE HEIGHT (ft)		
			Incident	Reflected	Transmitted
1 Dec 70	High (0800)	13.5	1.54	1.0	0.21
17 Dec 70	High (1330)	14.3	2.50	1.46	0.29
1 Dec 70	Low (2000)	14.3	1.33	0.80	0.09
1 Dec 70	Low (2330)	14.3	1.28	0.75	0.13
2 Dec 70	Low (2030)	14.3	1.51	0.93	0.18
14 Dec 70	Low (1600)	12.2	1.15	0.62	0.08

Note: (1) Condition of incipient wave overtopping of breakwater occurred at both the high tide conditions.

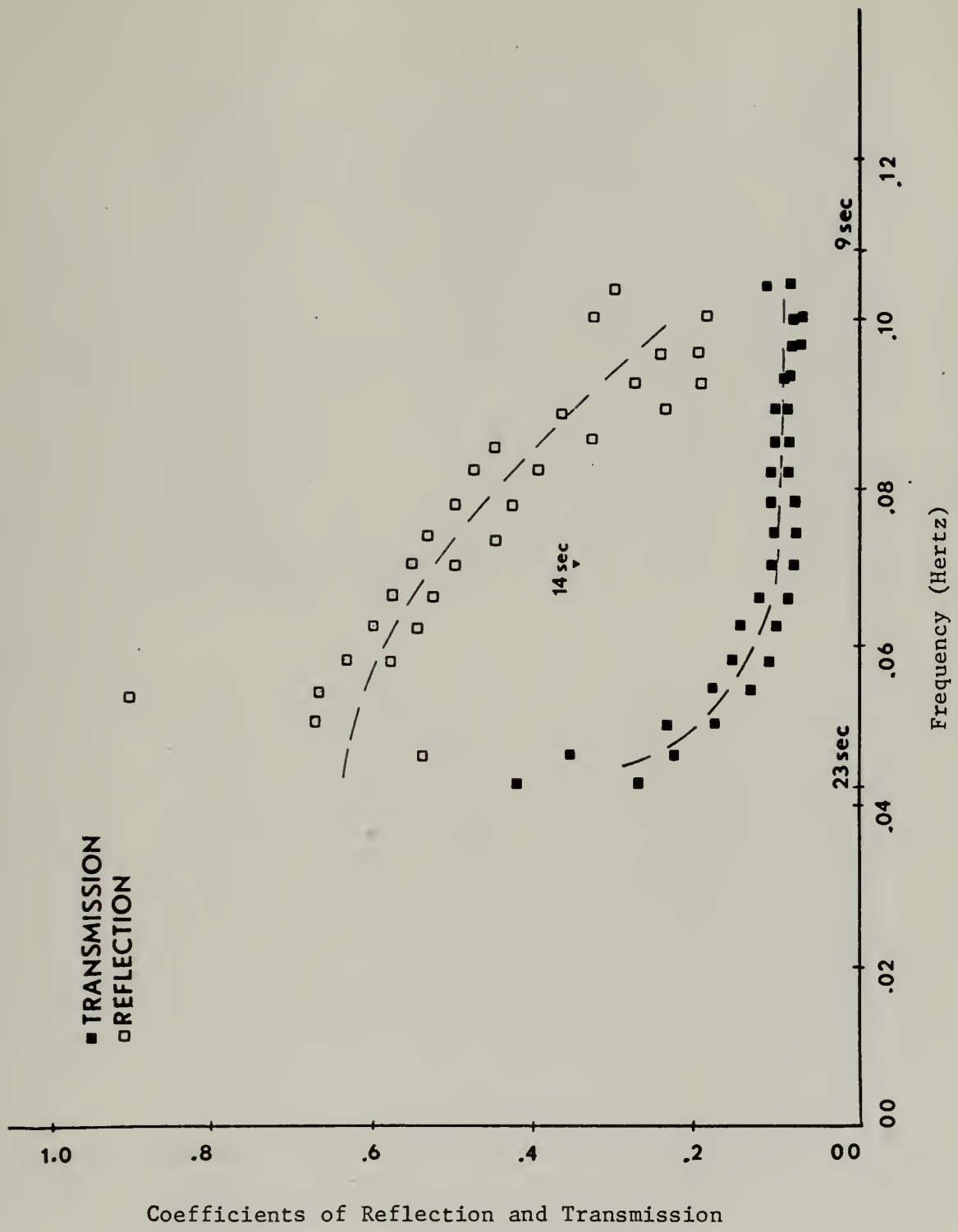

FIGURE 37

Coefficients of Reflection and Transmission, High Tide Conditions

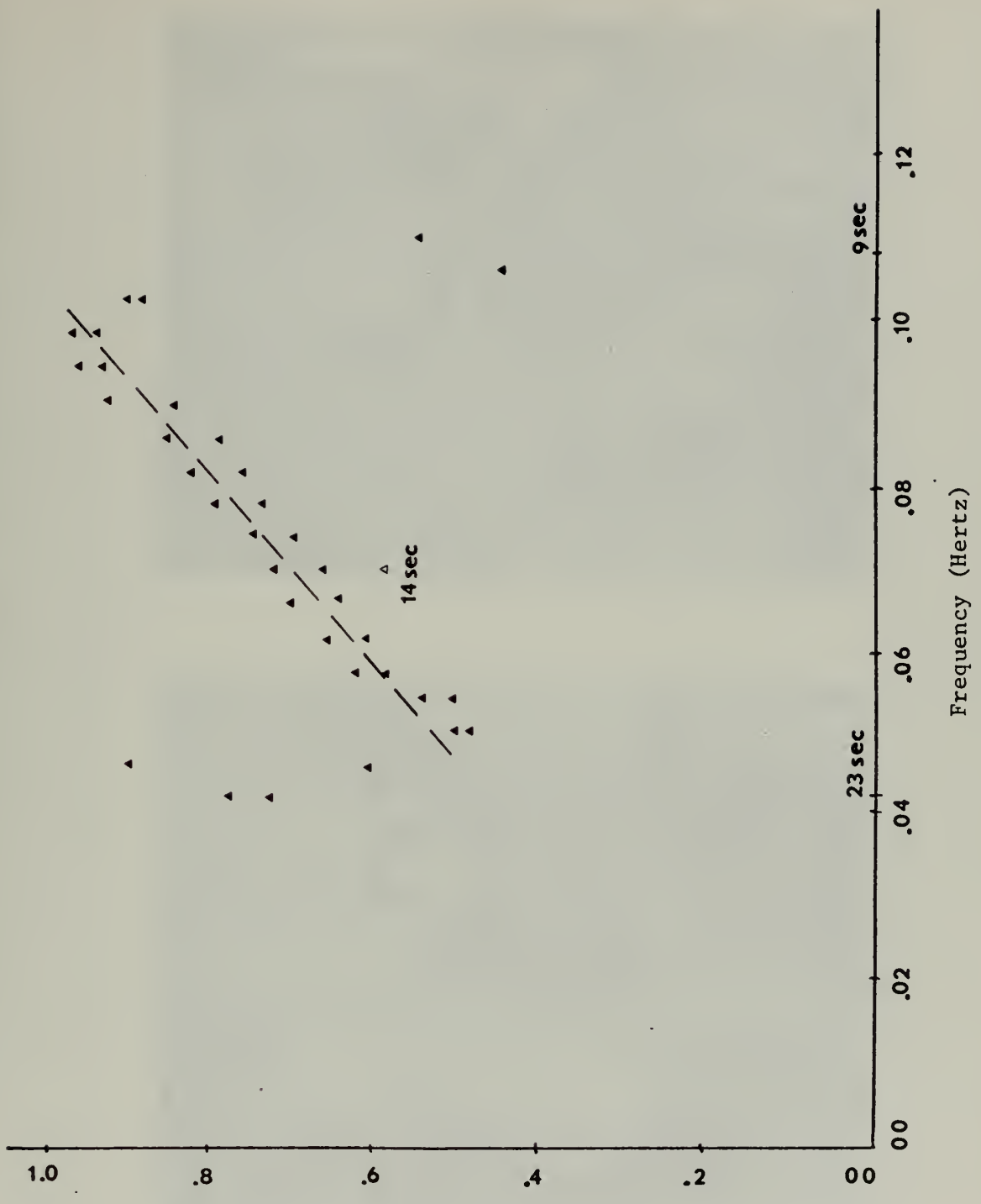

FIGURE 38

Coefficients of Energy Dissipation, High Tide Conditions

FIGURE 39

Breakwater at High Tide, 1 December 1970

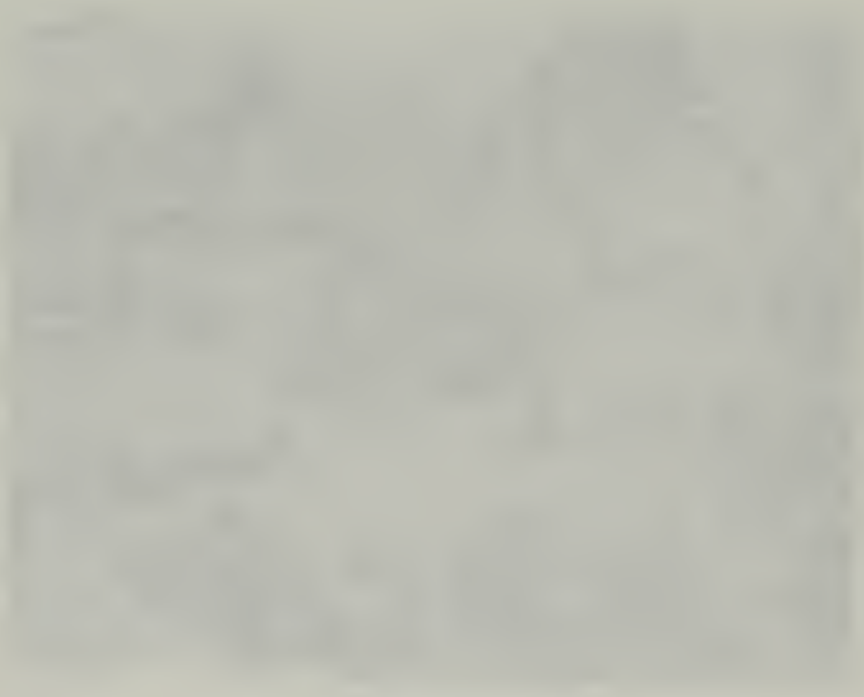

FIGURE 40

Breakwater at High Tide, 17 December 1970

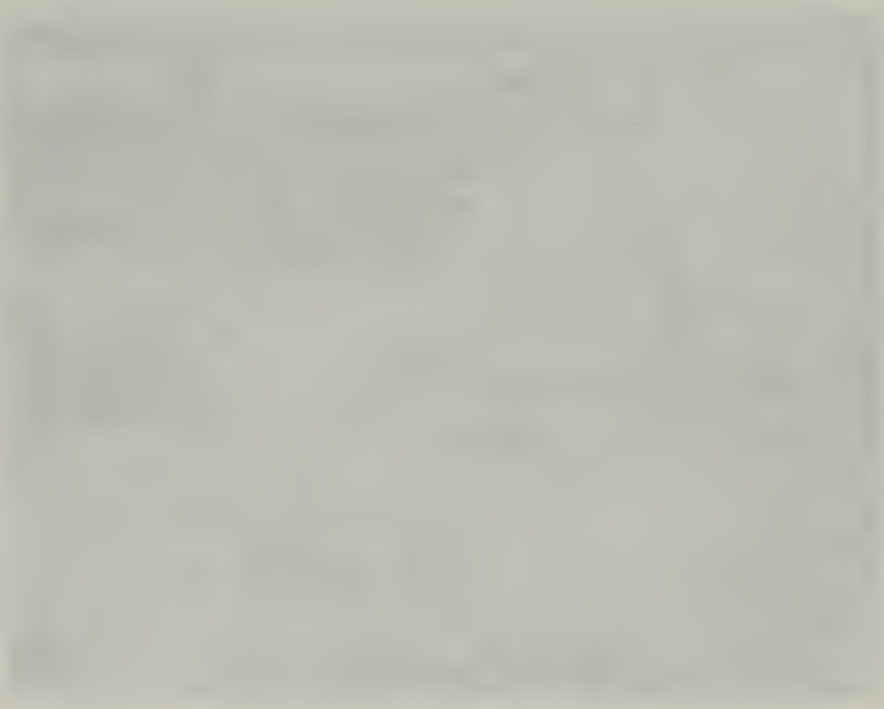

rubble-mound structure, increases consistently with an increase in frequency, noticeably counter to the decreasing reflection coefficient.

The reflection coefficient appears clearly related to the frequency variable. The coefficient of reflection occurring at the frequency of peak energy concentration, 0.071 Hz (14 sec) is approximately 0.50. The shape of the best-fit curve to the transmission coefficient values does not lend itself to a meaningful average value, although a coefficient of 0.10 at the frequency of peak energy concentration is representative of the sea and swell energy. A value of approximately 0.70 occurs for the energy dissipation coefficient at the frequency of peak energy concentration.

Figures 41 and 42 describe the coefficients at low tide conditions (average one foot MLLW) for four selected time-series records (Table I). No wave overtopping of the breakwater occurred on any of these occasions (Figure 43). Interpretation of these records is not as clear cut as for the high tide conditions. Data scatter was somewhat more prevalent and not as closely confined to the boundaries of the spectral frequency range of interest, 0.11 Hz (9 sec) and 0.044 Hz (23 sec).

The coefficient of reflection may be seen to reach a maxima at a frequency of 0.08 Hz. A reason as to this non-linear reflection curve (Figure 41) is a direct consequence of the structural condition of the breakwater. The exposed seaward slope has altered its configuration to a small degree and not uniformly. Rubble structures over the years will follow a process of disintegration; that is, wearing away, or dislodging stone by stone, rather than substantial collapse. This pseudo altered structure actually forms a more stable base. The portion of the breakwater more frequently exposed to attack by high breaking waves and the

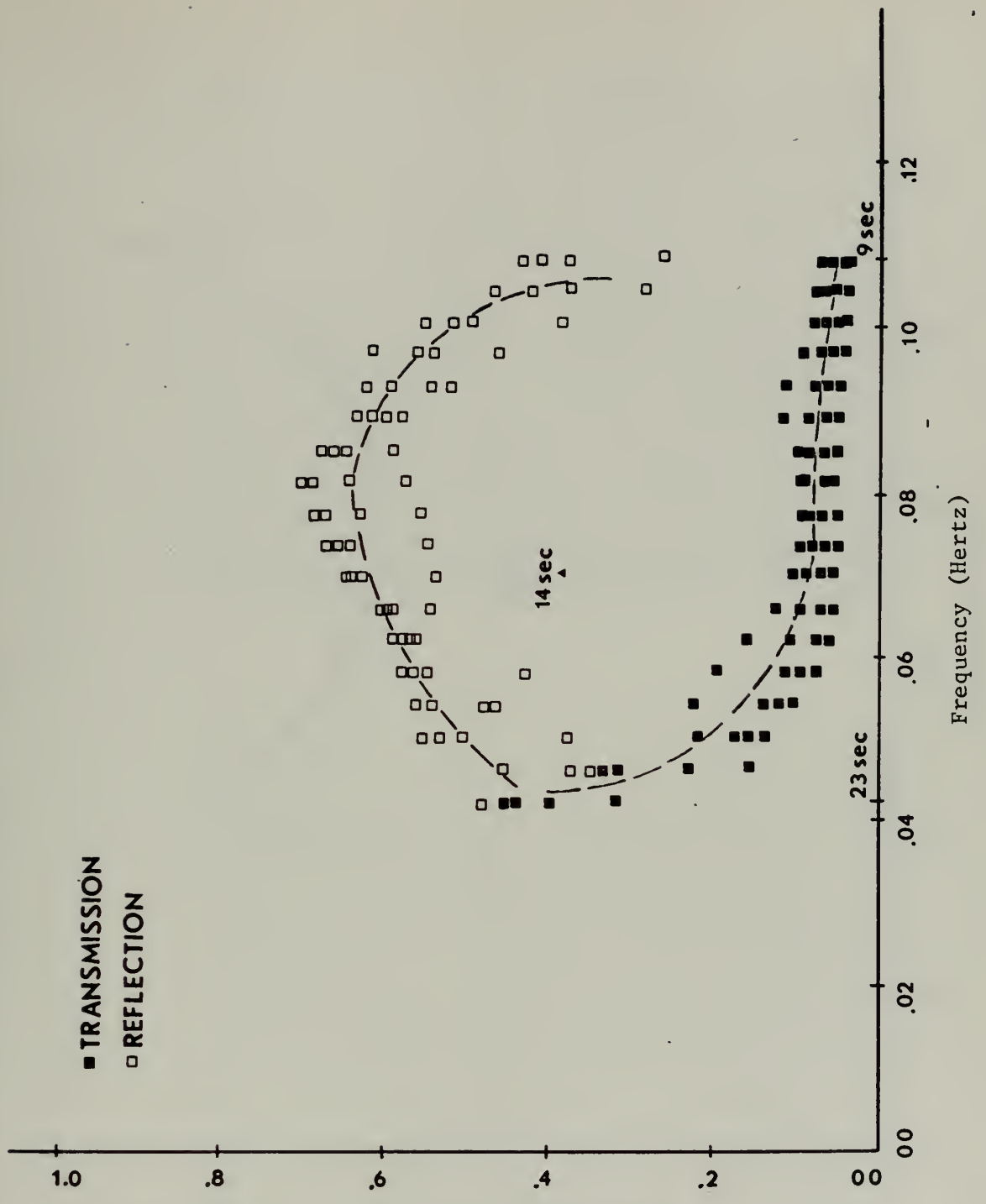

FIGURE 41

Coefficients of Reflection and Transmission, Low Tide Conditions

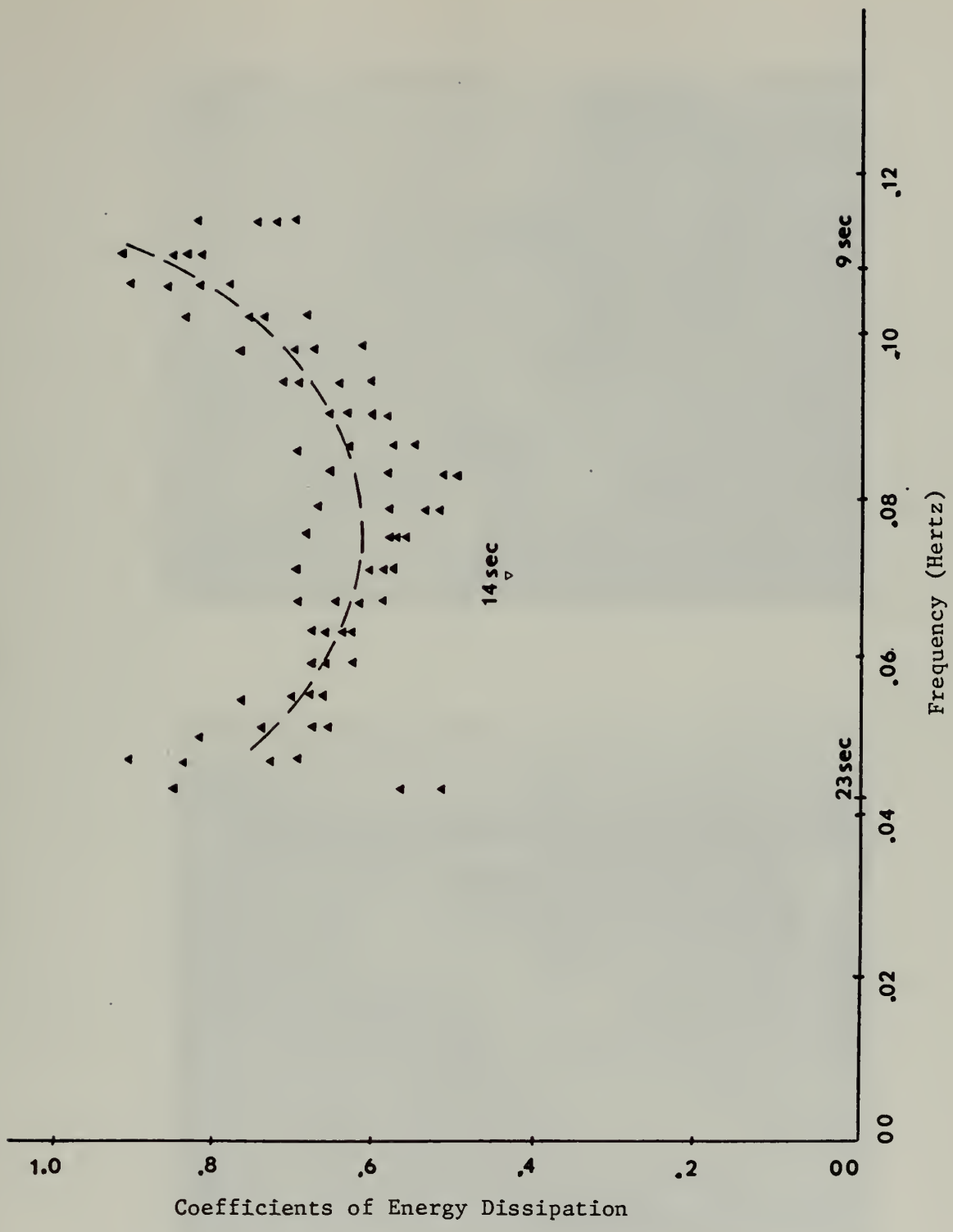

FIGURE 42

Coefficients of Energy Dissipation, Low Tide Conditions

FIGURE 43

Breakwater at Low Tide, 14 December 1970

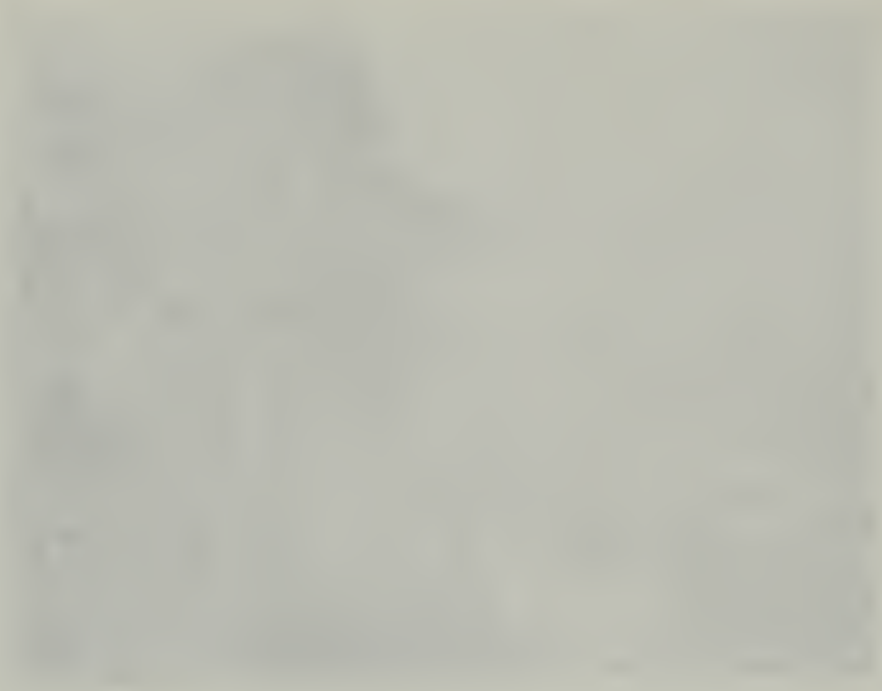

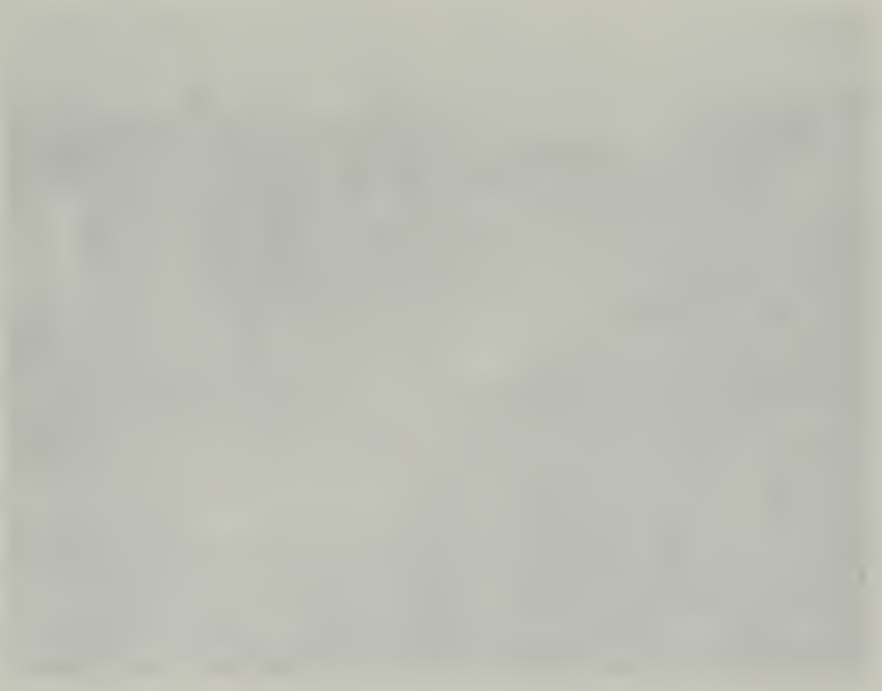

surge through the permeable structure lies in the upper section of the exposed breakwater. It is evident that the Monterey Breakwater has had armor stones dislodge from the upper section and subsequently settle along the breakwater slope in the lower section of the exposed breakwater. This has resulted in a decrease in slope on the seaward side to provide less verticality to incident wave energy. At low tide conditions, the higher energy wave components near the 14-second period band are incident to a greater extent on the more vertical section of the breakwater face higher up the slope and subsequently have a higher reflection coefficient. The lower energy wave components on both sides of the period of maximum energy concentration are dissipated and scattered to a larger extent by the greater number of less vertical angular reflecting surfaces along the direction of sea and swell incidence. The higher frequency energy components are scattered to an even greater degree due to their shorter wave lengths with considerable reduction in reflection coefficient.

A reflection coefficient of approximately 0.60 occurs at the frequency of peak energy concentration, 0.071 Hz (14 sec), and is slightly higher than the high tide conditions. This is presumably due to the absence of any wave overtopping as well as to the unique reflective considerations just discussed. The coefficient of transmission is similar in trend but a little lower in magnitude compared to the high tide conditions, having a constant coefficient of approximately 0.08 at frequencies above about 0.06 Hz. The smaller value of the coefficient is due to the denser packing of the rubble units in the lower section of the breakwater. The energy dissipation coefficient is similar to that for the high tide conditions in that it is also inversely related to

the reflection coefficient. A value of approximately 0.60 for the energy dissipation coefficient occurs at the frequency of peak concentration of energy, 0.071 Hz (14 sec), and is slightly lower than the high tide conditions.

D. COMPARISON WITH MODEL STUDY

Tangible results regarding transmission characteristics through model permeable rubble-mound structures in past studies have generally been derived for monochromatic waves generated in flume-type wave tanks or extensive harbor models. These small-scale models are designed and operated, and the test results are converted to prototype dimensions on the basis of transference equations derived from Froude's model laws. In addition, to preserve accurate results, the model breakwaters are constructed geometrically similar to the prototype. Harbor model studies are generally built with distorted scales which have adverse effects on the accuracy of test results when subjected to sea and swell [Hudson and Moore, 1950]; therefore, wave transmission studies are carried out primarily in wave tanks or flumes.

A model test of Monterey Harbor was constructed on a 1:40-scale breakwater structure at the U. S. Army Engineer Waterways Experiment Station to determine wave transmission characteristics of a proposed rubble-mound breakwater [Davidson, 1969]. Measured heights of transmitted and incident waves for a simulated 15-second monochromatic wave are tabulated in Table II. The results of the wave transmission test show that in general, heights of the transmitted waves were from 25 to 40 per cent of those of the incident waves for waves up to incipient overtopping of the structure. For purposes of comparison, the model breakwater differed from the prototype rubble-mound structure in that

TABLE II

Monterey Harbor Wave Transmission Data
from Hydraulic Model Investigation
(after Davidson, 1969)

H_I INCIDENT WAVE HEIGHT (ft)	H_T TRANSMITTED WAVE HEIGHT (ft) MEASURED AT:	
	L/4	L/2
3.0	0.8	0.8
4.5	1.2	1.2
6.0	1.6	1.2
7.5	2.0	1.6
9.0	2.4	2.8
10.5	4.0	4.0

Note: (1) H_I is the height of the incident wave measured at the structure site before the structure was installed in the model.

(2) Significant overtopping occurred with H_I = 10.5 feet.

(3) Monochromatic wave period was 15 seconds (simulated).

(4) H_T was measured at distances of one-quarter wave length (L/4) and one-half wave length (L/2).

(5) Wave flume used was 119 feet long, 5 feet wide, and 4 feet deep.

it had a crest height of plus 14 feet MLLW (four feet higher) with 12-ton tribars for the outer cover layer. Transmitted wave heights, plotted in Figure 44, were measured at distances of one-half and one-quarter of a 15-second wave length from the breakwater centerline.

The prototype data in Table I are plotted in Figure 44 to offer a comparison between the field and hydraulic model measurements. The prototype breakwater has a crest height of ten feet MLLW, which accounts for near wave overtopping conditions at lower incident wave heights than for the hydraulic model study. The heights of transmitted waves were from 7 to 12 per cent of the incident waves for conditions up to and including incipient wave overtopping of the structure.

Diffraction effects for the prototype breakwater have not been taken into account up to this point in the analysis. During the periods of field measurement no waves due to diffraction were visually observed in the vicinity of sensor No. 3 (harbor). Appropriate diffraction diagrams designed for semi-infinite impermeable breakwaters indicate a diffraction coefficient of less than 0.10 for a 15-second wave at the location of sensor No. 3 [Corps of Engineers, 1961]. Laboratory diffraction tests have shown that the theoretical values of diffracted wave heights within the geometric shadow of a breakwater exceed the actual values by about ten per cent [Dunham, 1950]. It is the author's opinion, in consideration of the fact that the geographic location of the sensor is far within the geometric shadow and at a sharp angle from the breakwater tip (500 feet from the tip of the breakwater and approximately 80 degrees from the incident wave direction), that the validity of diffraction theory is suspect at the location of the harbor sensor. The diffraction coefficient is considered to be well under 0.10, probably approaching zero over the period range dealt with.

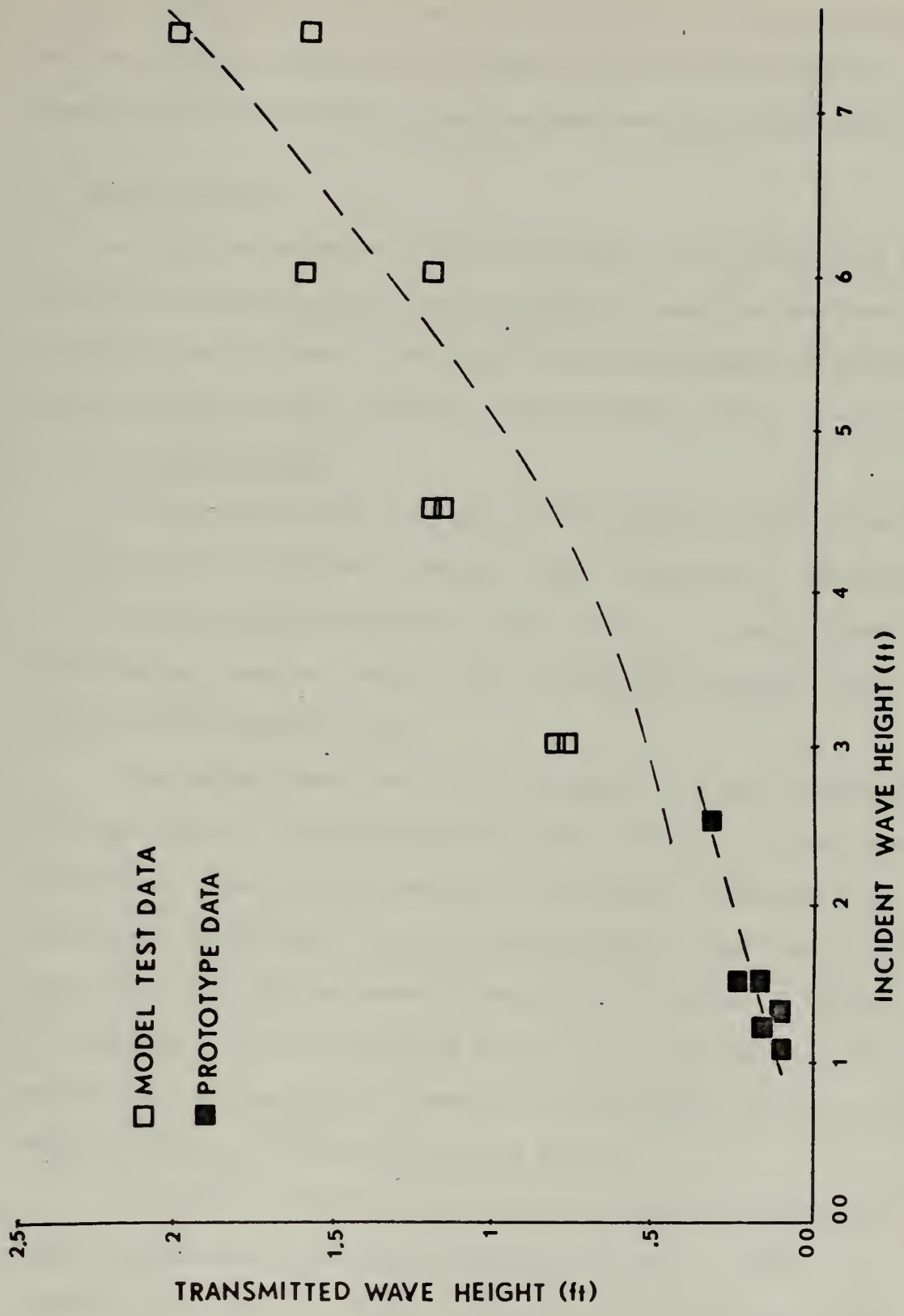

FIGURE 44

Transmitted Wave Heights for Protopype Study
and Hydraulic Model Investigation

As a consequence of discounting diffraction as contributing to the wave heights measured at the harbor sensor, the coefficients of transmission from the model studies appear even more conservative.

E. ERROR ANALYSIS

The errors encountered in this field study can be classified as either data-reduction, instrument location, or numerical-analysis oriented. Each of these error possibilities are examined below in order to determine their effect on the calculated results of this study.

1. Data Reduction

Time-induced errors may arise from synchronization of the wave records which is critical to spectral phase computation. The recording of the raw wave data from the two seaward sensors on analog traces was simultaneously done on a multi-channel recording instrument, which insures exact synchronization.

The harbor sensor (No. 3) was recorded as a curvilinear trace but digitized by a Calma 480 digitizer which accepts only rectilinear coordinates. The digitized data were subsequently reconverted to curvilinear coordinates. Linear interpolation was then used to match data points with the two seaward (sensors No. 1 and No. 2) records. The sampling interval was reduced from 0.80 to 0.63 seconds which maintained high resolution. Reduction and conversion of data in this manner resulted in very minor raw data errors.

A relation, obtained from linear wave theory, between wave height and recorded differential pressure was used to adjust the observed wave height according to wave frequency and sensor depth. Recent research by Bergan, Torum, and Traetteberg [1968] involving a comparison of wave measurements by a pressure-type wave gauge and

a continuous wire wave gauge found that the height difference of individual waves observed is significant. However, this same study confirms that the analysis of pressure gauge records of random sea waves gives reasonably accurate wave spectra and wave-height distributions. The agreement between significant wave heights obtained from the pressure and continuous wire gauge was within ten per cent. For the water depths and wave periods dealt with in this study, the error is considered well within ten per cent.

2. Instrument Location

The accuracy achieved in sensor positioning by transit and range line is considered within two feet. A bottom survey in the vicinity of the breakwater (Figure 4) was conducted by the author utilizing a portable fathometer with positioning fixed by transit, measuring tapes, and range lines. Depth accuracy was established within one foot. Therefore, errors in sensor positioning and bottom depth are considered to have negligible effect on the calculated results.

3. Numerical Analysis

The effect of approximating a finite time-series record with a step function and transforming the step function through computer spectral analysis can result in a number of misleading interpretations if not handled properly. Initially, this method of approximation by a step function can have considerable effect due to aliasing. Due to the high frequency cut-off and small sampling intervals of this study, aliasing, or the superposition of high frequency energy on the recorded wave form, is negligible.

Another source of numerical error is caused by the effect of transforming the record into discrete values of energy-density as a

function of discrete frequency bands. The energy is forced into certain band widths and centered about the middle frequency. In an effort to develop independent spectral amplitudes and modify any errors introduced, the records were smoothed by applying a Parzen tapered lag window to the auto-covariance function.

The assumption of an infinitely long record in theory and the use of a finite record in the analysis produces an error which can be expressed by confidence limits of the computed spectrum. The confidence limit is the probability that the true spectrum lies between the actual spectrum estimated from a finite sample. These bounds are a function of the number of degrees of freedom of the wave record, which is a function of record length and number of lags. To achieve the necessary balance between adequate resolution and reliable spectral density estimates, the number of lags was established at ten per cent of the total number of data points digitized (205 lags). This limited the number of degrees of freedom in each spectrum to 20 for each 21.5-minute time series. This, in turn, determined the confidence limits at the estimated power spectrum. For example, the 80 per cent confidence limits for 20 degrees of freedom are interpreted as meaning that one can state with 80 per cent accuracy that the true spectral estimate is greater than 0.71 but less than 1.60 at the actual power spectrum, as the spectrum is distributed according to chi-square distribution [Jenkins and Watts, 1969].

VI. CONCLUSIONS AND SUMMARY

The conclusions drawn from this field study are summarized as follows:

A. The method of resolving incident and reflected wave heights for a partial standing wave through the use of two fixed wave sensors was for the most part successful. The basic drawback was the inability to perform high frequency analysis in the period range of nine seconds and less. If the sensors had been positioned with a greater separation, the double nodal condition would have been displaced toward higher frequencies. The use of three sensors instead of two to seaward of the breakwater would have served the same purpose to resolve the incident and reflected waves in frequency bands above nine seconds.

B. The treatment of the wave transmission problem as a linear, stationary, random process is considered a reliable and useful technique. Power spectra complimented with cross spectral correlation resolved the wave field to seaward of the breakwater into incident and reflected spectral components. Confidence bounds of 0.71 and 1.60 for a confidence interval of 80 per cent were realized using a record length of 2048 data points with a maximum number of 205 lags.

Increased record length with a decrease in the ratio of number of lags to data points would have satisfied the requirements of good resolution and improved the confidence bounds. Whereas the sampling interval was fixed, the record length and number of lags were arbitrarily determined.

Coherence was lower in the high frequency domain, and is considered a result of the multi-directional scattering effect of incident waves

by the rough, angular, reflecting surfaces of the rubble-mound breakwater.

C. The transmission, reflection, and energy dissipation coefficients calculated from the prototype data followed the trends generally expected for wave energy incident on a rubble-mound breakwater. For high tide conditions, the reflection coefficient decreased linearly with increasing frequency. The energy-dissipation coefficient increased with increasing frequency in contrast to the reflection coefficient. The transmission coefficient was found to be approximately constant from the high frequency cut-off of 0.11 Hz (9 sec) to about 0.067 Hz (15 sec) where it increased abruptly with decreasing frequency. Coefficients of 0.10 for transmission, 0.50 for reflection, and 0.70 for energy dissipation occurred at the frequency of peak energy concentration, 0.071 Hz (14 sec). At low tide conditions, the coefficients were slightly different. The approximate reflection coefficient was slightly higher; the transmission coefficient lower, and the energy dissipation coefficients less than the high tide conditions.

D. The numerical results obtained from the prototype transmission tests and from the proposed Monterey Breakwater model did not agree particularly well. For the hydraulic model study, the heights of transmitted waves were reported to be from 25 to 40 per cent of those of the incident waves, whereas the prototype field measurements were from 7 to 12 per cent within the same general frequency range and with no significant wave overtopping. It is important to note that significant wave height is the height parameter used in the prototype transmission study; whereas, the actual heights of the monochromatic waves

were used in the hydraulic laboratory investigation. The possibility remains that the model laws of similarity for prototype scaling and the effect of artificially generated waves produce over-estimated results. It may be concluded from this study of the Monterey Harbor breakwater that the design of rubble-mound breakwaters in general, based on model studies of wave energy transmission, may be conservative.

REFERENCES

1. Bergan, P. O., A. Torum, and A. Traetteberg, 1968. "Wave Measurements by a Pressure Type Wave Gauge." Proc. Eleventh Conference on Coastal Engineering, London, England.

2. Bixby, H. L., 1962. Storms Causing Harbor and Shoreline Damage Through Wind and Waves Near Monterey, California. Naval Postgraduate School, Monterey, California, M.S. Thesis.

3. Blackman, R. B. and J. W. Tukey, 1958. The Measurement of Power Spectra. Dover Publications, Inc., New York, New York.

4. Bucci, D. R. and R. W. Whalin, 1969. Runup Characteristics of Explosion-Generated Waves in Major Harbor Areas, Report No. 1: Wave Intrusion into Monterey Harbor, California. Technical Report N-69-4, Waterways Experiment Station, Vicksburg, Mississippi, U. S. Army Corps of Engineers.

5. Chatham, C. E., 1968. Wave and Surge Conditions after Proposed Expansion of Monterey Harbor, Monterey, California. Technical Report H-68-9, Waterways Experiment Station, Vicksburg, Mississippi, U. S. Army Corps of Engineers.

6. Corps of Engineers, U. S. Army, 1961. Shore Protection Planning and Design. Technical Report No. 4, Beach Erosion Board, Washington, D. C.

7. Davidson, D. D., 1969. Stability and Transmission Tests of Tribar Breakwater Section Proposed for Monterey Harbor, California. Miscellaneous Paper H-69-11, Waterways Experiment Station, Vicksburg, Mississippi, U. S. Army Corps of Engineers.

8. Dean, R. G., 1968. "Relative Validities of Water Wave Theories." Proc. Civil Engineering in the Oceans, ASCE.

9. Dunham, J. W., 1950. "Refraction and Diffraction Diagrams." Proc. First Conference of Coastal Engineering, Long Beach, California.

10. Hudson, R. Y., 1949. Wave and Surge Action, Monterey Harbor, Monterey, California. Technical Memorandum No. 2-301, Waterways Experiment Station, Vicksburg, Mississippi, U. S. Army Corps of Engineers.

11. Hudson, R. Y. and L. F. Moore, 1950. "The Hydraulic Model as an Aid in Breakwater Design." Proc. First Conference on Coastal Engineering, Long Beach, California.

12. Jenkins, G. M. and D. G. Watts, 1969. Spectral Analysis and Its Applications. Holden-Day, San Francisco, California.

13. Lynch, J. L., 1970. Long Wave Study of Monterey Bay. Naval Postgraduate School, Monterey, California, M.S. Thesis.

14. National Marine Consultants, 1960. Wave Statistics for Seven Deep Water Stations Along the California Coast. National Marine Consultants, Inc., Santa Barbara, California.

INITIAL DISTRIBUTION LIST

		No. Copies
1.	Defense Documentation Center Cameron Station Alexandria, Virginia 22314	2
2.	Library, Code 0212 Naval Postgraduate School Monterey, California 93940	2
3.	Oceanographer of the Navy The Madison Building 732 N. Washington Street Alexandria, Virginia 22314	1
4.	Department of Oceanography, Code 58 Naval Postgraduate School Monterey, California 93940	3
5.	Dr. E. B. Thornton, Code 58Tm Department of Oceanography Naval Postgraduate School Monterey, California 93940	3
6.	Dr. W. C. Thompson, Code 58Th Department of Oceanography Naval Postgraduate School Monterey, California 93940	1
7.	LCDR Ronald J. Calhoun, USN 7701 Manet Parkway Sacramento, California 93923	3
8.	Chief of Naval Research Geography Programs, Code 414 Office of Naval Research Washington, D. C. 20360	1
9.	Commanding Officer Office of Naval Research Branch Office Box 39 Fleet Post Office New York, New York 09510	1
10.	Chief of Naval Research Ocean Science and Technology Group Code 480 Office of Naval Research Washington, D. C. 20360	1

11. Commander — 1
Naval Facilities Engineering Command
Engineering & Design
Washington, D. C. 20390

12. Waterways Experiment Station — 1
U. S. Corps of Engineers
Vicksburg, Mississippi 39180
Attn: Head, Research Center Library

13. Commanding Officer — 1
U. S. Army, Corps of Engineers
North Pacific Division Office
San Francisco, California 94102
Attn: Mr. Orville T. Magoon

14. Commanding Officer — 1
U. S. Army, Corps of Engineers
San Francisco District Office
100 McAllister Street
San Francisco, California 94102
Attn: Mr. Bob Sloan

15. Dr. Douglas L. Inman — 1
Scripps Institute of Oceanography
University of California, San Diego
P. O. Box 109
La Jolla, California 92038

16. Prof. Joe Johnson — 1
Department of Civil Engineering
412 Hesse Hall
University of California, Berkeley
Berkeley, California 94700

17. Mr. Thorndike Saville, Jr., Director — 1
Research Division
Coastal Engineering Research Center
520 Little Falls Road, N.W.
Washington, D. C. 20016

18. Dr. R. G. Dean — 1
Coastal and Oceanographic Engineering Department
University of Florida
Gainesville, Florida 32601

19. Mr. V. J. Grauzinis — 1
The Bisset-Berman Corporation
3939 Ruffin Road
San Diego, California 92123

Security Classification

DOCUMENT CONTROL DATA - R & D

(Security classification of title, body of abstract and indexing annotation must be entered when the overall report is classified)

1. ORIGINATING ACTIVITY (Corporate author)	2a. REPORT SECURITY CLASSIFICATION
Naval Postgraduate School Monterey, California 93940	Unclassified
	2b. GROUP

3. REPORT TITLE

Field Study of Wave Transmission Through a Rubble-Mound Breakwater

4. DESCRIPTIVE NOTES (Type of report and, inclusive dates)

Master's Thesis: March 1971

5. AUTHOR(S) (First name, middle initial, last name)

Ronald Joel Calhoun

6. REPORT DATE	7a. TOTAL NO. OF PAGES	7b. NO. OF REFS
March 1971	88	14

8a. CONTRACT OR GRANT NO.	9a. ORIGINATOR'S REPORT NUMBER(S)
b. PROJECT NO.	
c.	9b. OTHER REPORT NO(S) (Any other numbers that may be assigned this report)
d.	

10. DISTRIBUTION STATEMENT

Approved for public release; distribution unlimited

11. SUPPLEMENTARY NOTES	12. SPONSORING MILITARY ACTIVITY
	Naval Postgraduate School Monterey, California 93940

13. ABSTRACT

Characteristics of sea and swell incident at a permeable rubble-mound breakwater located in Monterey Harbor, California, are resolved into reflected and transmitted components. The wave characteristics are studied by analyzing synchronized wave records of three underwater sensors judiciously placed, two to seaward and one to landward of the breakwater. Power spectra and cross spectra are calculated for various characteristic sea states selected from three months of observations. Amplitude and phase are determined for the spectral wave components comprising the partial standing wave pehnomena. This study was unique in that it entails experiments conducted in the field on a prototype structure in the natural environment. Transmission has been studied heretofore exclusively with scale models. The coefficients of transmission are considerably less for the prototype than predicted by a Corps of Engineers model study of the Monterey Breakwater. The differences are apparently related to more wave energy scattering and dissipation due to turbulence than predicted by the model.

DD FORM 1 NOV 65 1473 (PAGE 1)

S/N 0101-807-6811

Security Classification

A-31408

14. KEY WORDS	LINK A		LINK B		LINK C	
	ROLE	WT	ROLE	WT	POLE	WT
Partial Standing Wave						
Wave Transmission Through Breakwater						
Breakwater Design						
Field Study Rubble-Mount Breakwater						
Monterey Harbor						

DD FORM 1 NOV 65 1473 (BACK)

S/N 0101-807-6821

Thesis
C187
c.1

126554

Calhoun
Field study of wave transmission through a rubble-mound breakwater.